Molecular Therapy
Original Article

Urinary Extracellular Vesicles Carrying Klotho Improve the Recovery of Renal Function in an Acute Tubular Injury Model

Cristina Grange,[1,4] Elli Papadimitriou,[2,4] Veronica Dimuccio,[2] Cecilia Pastorino,[2] Jordi Molina,[2] Ryan O'Kelly,[3] Laura J. Niedernhofer,[3] Paul D. Robbins,[3] Giovanni Camussi,[1] and Benedetta Bussolati[2]

[1]Department of Medical Sciences, University of Turin, Turin, Italy; [2]Department of Molecular Biotechnology and Health Sciences, University of Turin, Turin, Italy; [3]Institute on the Biology of Aging and Metabolism, Department of Biochemistry, Molecular Biology and Biophysics, University of Minnesota Medical School, Minneapolis, MN, USA

Acute kidney injury, defined by a rapid deterioration of renal function, is a common complication in hospitalized patients. Among the recent therapeutic options, the use of extracellular vesicles (EVs) is considered a promising strategy. Here we propose a possible therapeutic use of renal-derived EVs isolated from normal urine (urine-derived EVs [uEVs]) in a murine model of acute injury generated by glycerol injection. uEVs accelerated renal recovery, stimulating tubular cell proliferation, reducing the expression of inflammatory and injury markers, and restoring endogenous Klotho loss. When intravenously injected, labeled uEVs localized within injured kidneys and transferred their microRNA cargo. Moreover, uEVs contained the reno-protective Klotho molecule. Murine uEVs derived from Klotho null mice lost the reno-protective effect observed using murine EVs from wild-type mice. This was regained when Klotho-negative murine uEVs were reconstituted with recombinant Klotho. Similarly, ineffective fibroblast EVs acquired reno-protection when engineered with human recombinant Klotho. Our results reveal a novel potential use of uEVs as a new therapeutic strategy for acute kidney injury, highlighting the presence and role of the reno-protective factor Klotho.

INTRODUCTION

Acute kidney injury (AKI), a common complication in hospitalized patients, is characterized by a rapid deterioration of renal function.[1] Around 8%–16% of the patients suffering from AKI are estimated to progress to chronic renal disease, with high mortality risk and related costs.[2–4] Although the renal tissue shows an intrinsic ability to regenerate after damage, full recovery in most of the cases is not achieved. Therefore, multiple clinical approaches for renal regeneration are nowadays being considered.

Among the new therapeutic options for AKI, the use of stem cell-derived extracellular vesicles (EVs) is gaining increasing interest.[5] For example, EVs from mesenchymal stromal cells (MSC EVs) have been found to exert a promising therapeutic effect.[6–12] MSC EVs may act through multiple regenerative processes, including induction of tubular cell survival, proliferation, suppression of inflammation, and inhibition of fibrosis.[7–9,13] The transfer of EV biological cargo (proteins, RNAs, and DNAs) into target cells appears fundamental in cell fate modulation.[14–16] Interestingly, microRNAs (miRNAs), transferred by MSC EVs, have been considered the main effectors in the enhancement of proliferation and survival of renal tubular cells.[9,14]

Renal cells lining the nephron also release bioactive EVs able to target downstream cells, suggesting the presence of an intranephron communication between cells along the urinary lumen.[17,18] EVs released by proximal tubular cells were shown to be internalized by distal tubule and collecting duct cells *in vitro*.[19] Moreover, in collecting duct cells, the functional transfer of AQP2 via EVs has been reported.[20] Urine-derived EVs (uEVs) have been extensively characterized for their cargo[21–24] and found to contain kidney cell-specific markers from different nephron segments, such as megalin, cubilin, aminopeptidase, aquaporin-1 (AQP1), aquaporin-2 (AQP2), podocin, and podocalyxin (PDX).[25] Indeed, EVs, present in the urine, are considered to mainly derive from renal cells rather than serum, considering the small size (6-nm diameter) of renal filtration pore.[26] However, the potential role of uEVs in renal recovery after damage is currently unknown. Interestingly, a proteomic analysis revealed that uEVs contain Klotho,[21,22] a single-pass transmembrane protein crucial in renal tissue regeneration.[27] Klotho was initially identified as an anti-aging gene,[28] highly expressed in the kidney.[29] The protein's extracellular domain, when cleaved, is released into the circulation and acts as a soluble factor, exerting a reno-protective role in tissue regeneration.[30–34] Klotho is modulated within renal

Received 21 June 2019; accepted 7 November 2019;
https://doi.org/10.1016/j.ymthe.2019.11.013.

[4]These authors contributed equally to this work.

Correspondence: Benedetta Bussolati, Department of Molecular Biotechnology and Health Sciences, University of Turin, via Nizza 52, 10126 Turin, Italy.
E-mail: benedetta.bussolati@unito.it

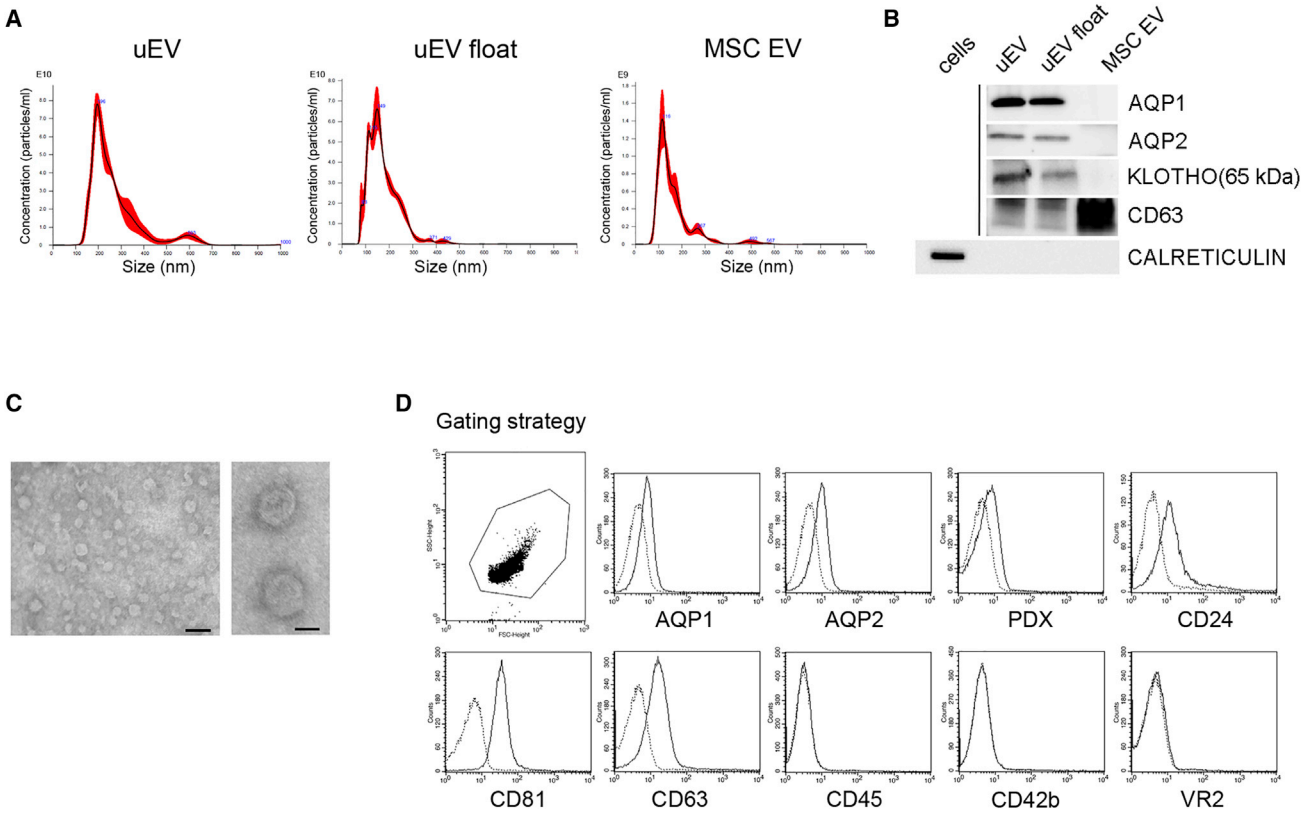

Figure 1. EV Characterization

(A) NanoSight representative images of uEVs isolated by ultracentrifuge (uEV) and floating (uEV float) protocols and of MSC EVs. (B) Representative western blot showing renal and exosomal markers AQP1, AQP2, Klotho, CD63, and calreticulin in uEVs, uEVs float, and MSC EVs; calreticulin expression by fibroblast cells was analyzed as positive control. Three different uEV preparations were analyzed with similar results. (C) Representative micrographs of transmission electron microscopy obtained from purified uEVs (scale bars: right panel, 50 nm; left panel, 200 nm). (D) Representative cytofluorimetric analyses of uEVs showing the positive expression of renal and exosomal markers AQP1, AQP2, PDX, CD24, CD81, CD63, and the negative expression of monocyte, platelet, and endothelial markers CD45, CD42b, and VEGFR2 (VR2), respectively. Dotted line histograms specify isotypic controls. Three different uEV preparations were analyzed with similar results.

tissue after injury, and its levels decline in blood, urine, and kidney in acute[31] and chronic damage.[32,33] On the other side, forced expression of exogenous Klotho has been shown to exert a reno-protective role, indicating that Klotho administration can be considered as a promising approach for kidney repair.[34,35]

The aim of the present study is to investigate the possible therapeutic use of human uEVs in the recovery of renal damage in an experimental model of AKI, generated by glycerol injection. Moreover, the specific role of the reno-therapeutic factor Klotho, present in EV cargo, is dissected.

RESULTS

Effect of uEVs on the Recovery of AKI

To determine whether uEVs have therapeutic action, the effect of uEVs was evaluated in a murine model of rhabdomyolysis-induced AKI.[8] This model is characterized by muscle injury and the subsequent release of nephrotoxic substances and iron deposition on renal tissue (Figure S1). uEVs were obtained by ultracentrifugation of urine from healthy volunteers (n = 25 different pools). In selected experiments, uEVs were further purified by floating on density gradient (uEV float), to exclude the effect of non-vesicular contaminants.[36] The mean diameter of uEVs and uEVs float was 175.1 ± 69 nm (mode: 149 ± 30 nm) and 160.1 ± 34 nm (mode: 150 ± 28 nm), respectively, as evaluated by NanoSight analysis (Figure 1A). The identity of the EVs was confirmed by the expression of CD63 and lack of calreticulin, an endoplasmic reticulum marker (Figure 1B). Moreover, transmission electron microscopy of uEVs demonstrated their spheroid morphology and confirmed their size in the nano-range (Figure 1C). EVs from urine expressed the characteristic renal markers AQP1, AQP2, and Klotho, absent in MSC EVs used as a control (Figure 1B). Moreover, cytofluorimetric analyses of uEVs confirmed the presence of renal tubular and podocyte surface markers (AQP1, AQP2, and PDX), as well as of renal exosomal markers (CD24,[37] CD81, and CD63). No detection of markers of platelets, endothelial cells, and monocytes/leukocytes, reported in serum EVs,[38] was observed (Figure 1D).

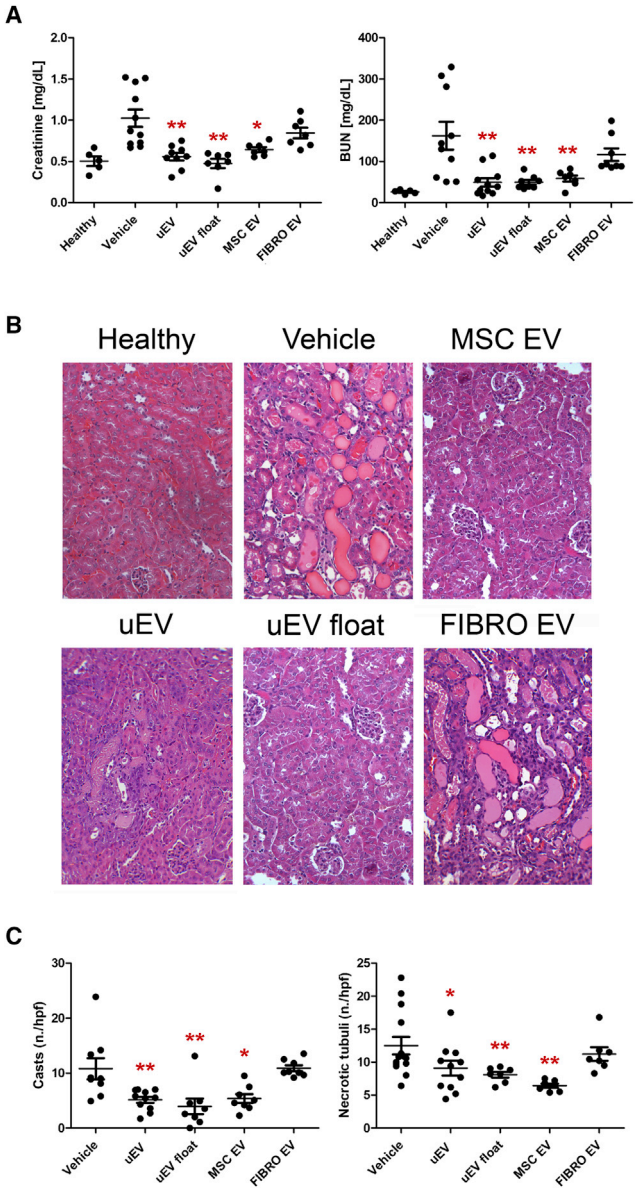

Figure 2. uEVs Improve Renal Recovery in an AKI Mouse Model

(A) Alterations in renal function were assessed by evaluating creatinine and BUN levels at day 3 after damage. Mice treated with uEVs (at least five different pools), isolated by both ultracentrifuge (uEV) and floating (uEV float) protocols, showed significantly reduced levels of creatinine and BUN compared with untreated AKI mice (vehicle). Similar amelioration was observed in mice treated with MSC EVs. No renal function improvement was observed using fibroblast EVs (FIBRO EVs). Data are expressed as the mean ± SEM of eight mice per group. ANOVA with Dunnett's multicomparison test was performed: *$p < 0.05$ or **$p < 0.001$ versus vehicle. (B) Representative micrographs of histological analysis (H&E staining) of renal tissue from healthy and AKI mice treated with saline (vehicle), uEVs, uEVs float, MSC EVs, and FIBRO EVs at day 3 after damage. Original magnification ×200. (C) Quantification of tubular hyaline casts and tubular necrosis at day 3 after damage. Data are expressed as the mean ± SEM. Ten fields per section were analyzed. ANOVA with Dunnett's multicomparison test was performed: *$p < 0.05$ or **$p < 0.001$ versus vehicle.

One day after AKI induction, concomitant with the peak of the damage, mice received the following treatments: (1) uEVs, (2) uEVs float, (3) EVs from MSCs, and (4) EVs from fibroblasts. MSC and fibroblast EVs were used as positive and negative controls, respectively. All mice received 2.0×10^8 uEVs/100 μL (a reported effective dose for MSC EVs[14]) into the tail vein. The control group was treated with 100 μL of saline (vehicle). Mice injected with uEVs and floating uEVs showed a significant reduction of blood urea nitrogen (BUN) and creatinine at day 3 (48 h after treatment) compared with untreated mice (Figure 2A). The amelioration in physiological parameters induced by uEVs was similar to that obtained by the administration of pro-regenerative MSC EVs (Figure 2A). In contrast, fibroblast EVs did not have any effect on the recovery (Figure 2A).

The histological evaluation of kidney sections in the vehicle group revealed the presence of intra-tubular protein casts and tubular epithelial cell necrosis (Figure 2B). Mice treated with uEVs or MSC EVs, but not with fibroblast EVs, showed preserved tissue architecture similar to that of healthy mice (Figure 2B). The number of casts and necrotic tubules was significantly reduced in uEV- and MSC EV-treated mice, confirming their beneficial effect (Figure 2C). No significant difference was observed between animals treated with uEVs and MSCs. On the same line, uEV and MSC EV treatments improved tubular cell proliferation (Figures 3A and 3B) and reduced tubular cell apoptosis (Figure S2) compared with the vehicle group. The pro-regenerative effect of uEVs was further confirmed by using float uEVs (Figures 2 and 3).

We further analyzed, at mRNA level, the effect of uEVs on markers of renal damage and inflammation. In particular, AKI mice showed an increased expression of renal injury markers such as NGAL, PAI, and caspase-3 (Figure 3C). Moreover, SOX9, a transcription factor induced in tubular cells as a consequence of tissue damage,[39] was also upregulated (Figure 3C). In contrast, mice treated with uEVs, as well as MSC EVs, showed a significant downregulation of injury markers (Figure 3C). In addition, renal tissue from AKI mice showed a significant increase of pro-inflammatory cytokines such as tumor necrosis factor alpha (TNF-α), interleukin-1β (IL-1β), and IL-6 (Figure 3D). The administration of uEVs prevented the inflammatory cascade in a manner similar to MSC EVs, with a significant reduction of all inflammatory markers analyzed (Figure 3D). Moreover, the pro-inflammatory driver nuclear factor κB (NF-κB) was significantly upregulated during AKI and downregulated by uEV treatment (Figure 3D).

uEV Localization and miRNA Cargo Transfer to Renal Injured Tissue

To determine the localization of uEVs within injured renal tissue, uEVs labeled with a fluorescent dye were injected intravenously and tracked by optical imaging in both healthy and AKI mice. The biodistribution analysis, performed 4 h after the administration of uEVs, revealed the presence of fluorescent signal in whole-body images, as well as in *ex vivo* isolated kidneys (Figure 4A). The

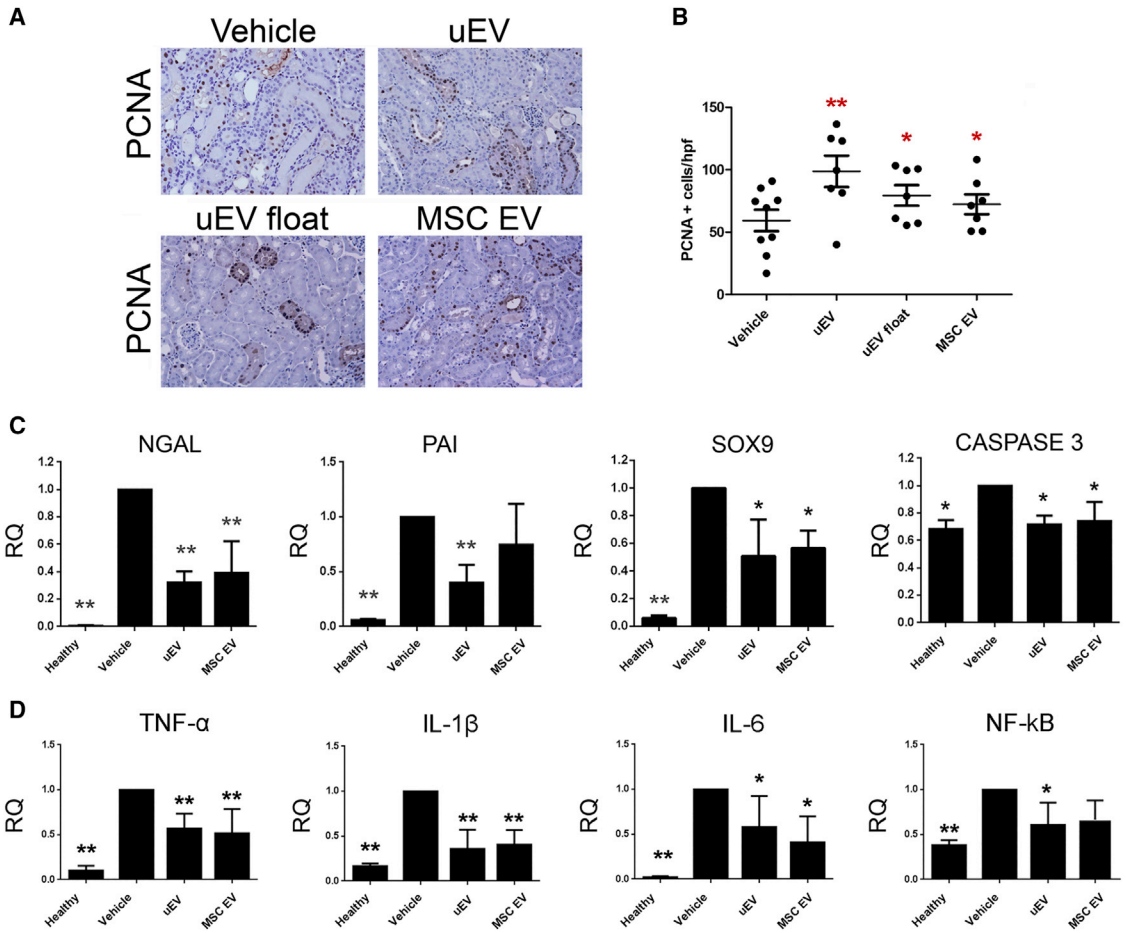

Figure 3. uEVs Stimulate Tubular Proliferation and Reduce Levels of Renal Injury and Inflammatory Markers

(A) Representative micrographs showing PCNA (Proliferating Cell Nuclear Antigen)-positive cells in kidney tissues from AKI mice injected with saline (vehicle), uEVs, uEVs float, and MSC EVs at day 3 after damage. Original magnification ×200. (B) Quantification of PCNA-positive cells in AKI mice treated with saline (vehicle) and EVs at day 3 after damage. Data are expressed as the mean ± SEM of the count of 10 fields/section (n = 8 mice for each group). ANOVA with Dunnett's multicomparison test was performed: *$p < 0.05$, **$p < 0.001$ versus vehicle. (C) Histograms showing mRNA expression represented by relative quantification (RQ) of NGAL, PAI, SOX9, and caspase-3 in healthy and AKI mice, treated with saline (vehicle), uEVs, and MSC EVs, at day 3 after damage. Data are normalized to GAPDH and to 1 for vehicle, and are expressed as the mean ± SEM of healthy (n = 3), vehicle, and EVs (n = 7/group). One-way ANOVA was performed: *$p < 0.05$ and **$p < 0.001$ versus vehicle. (D) Histograms showing the mRNA expression represented by relative quantification (RQ) of inflammatory markers TNF-α, IL-1β, IL-6, and NF-κB in healthy and AKI mice, treated with saline (vehicle), uEVs, and MSC EVs, at day 3 after damage. Data are normalized to GAPDH and to 1 for vehicle, and are expressed as the mean ± SEM of healthy (n = 3), vehicle, and EVs (n = 7/group). One-way ANOVA was performed: *$p < 0.05$ and **$p < 0.001$ versus vehicle.

fluorescence, acquired in live animals, was detectable in spleen and kidney of healthy and AKI mice. However, the injured kidneys showed higher fluorescent intensity compared with the healthy ones (Figure 4A). The analysis of dissected kidneys revealed the preferential uEV localization in damaged organs (Figure 4B).

To confirm the effective localization of uEVs into injured kidneys, we analyzed the transfer of their miRNA cargo to renal tissue. In particular, from the 204 miRNAs, identified by array within uEVs (Table S1), we confirmed the expression of the top 10 uEV miRNAs by quantitative real-time PCR, and we evaluated their transfer to renal tissue (Table S2; Figure 4C). We observed a significant increase of miR-30 family and miR-151 in renal tissue, 4 h after uEV injection, demonstrating the transfer of four uEV miRNAs to injured kidneys (Figure 4D). Predictive target analysis, using the FunRich tool, performed on the four highly expressed and transferred uEV miRNAs, showed 1,545 selectively predicted target genes. Subsequently, interactome network analysis was conducted to identify relevant pathways involved in uEV biological function (Figure S3). The analysis revealed a strong representation ($p < 0.001$) of molecules involved in pro-regenerative pathways, such as proteoglycan-syndecan signaling events, insulin growth factor 1 (IGF-1) and hepatocyte growth factor (HGF). The effect of EV cargo within the renal tissue was further confirmed by the downregulation of selected miRNA targets. In fact, SMAD1 and SMAD2, central factors in the interactome, cyclin D1 (CCND1) (miR-30a target), and c-Myc (miR-30 family and

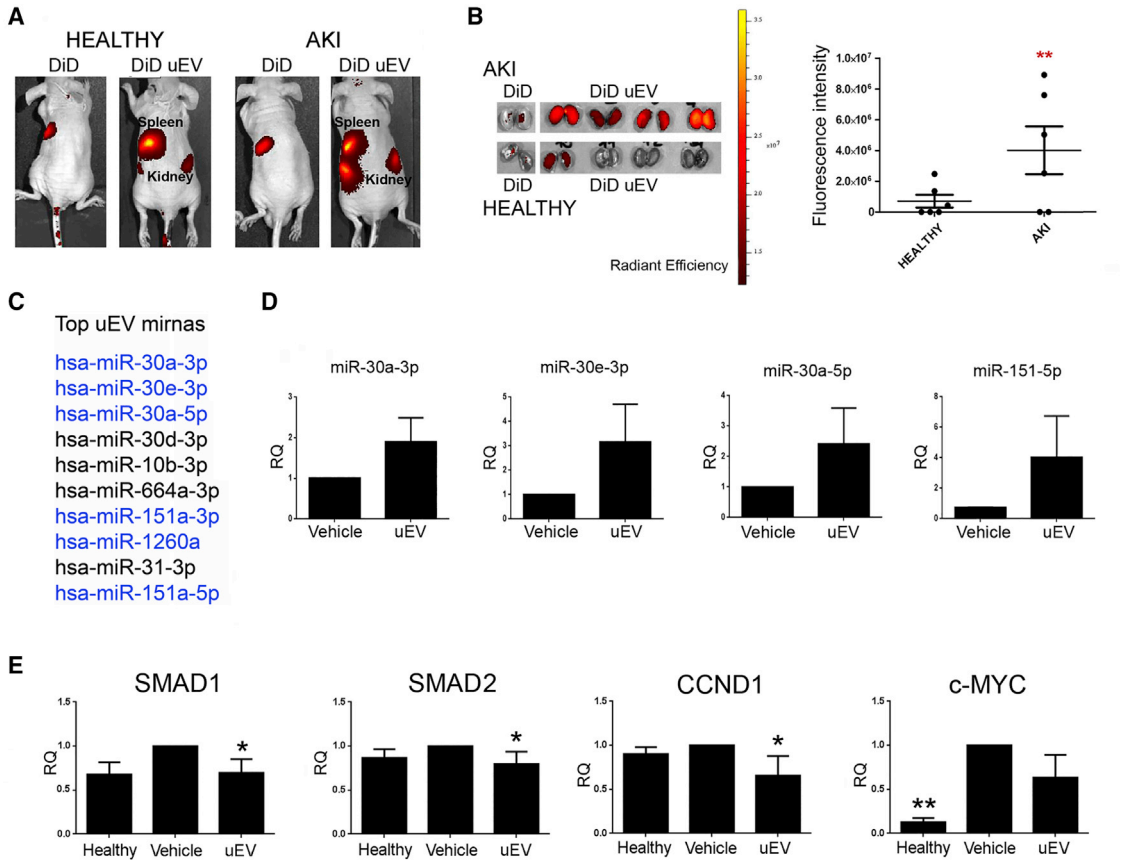

Figure 4. Localization of Labeled uEVs and miRNA Cargo Transfer

(A) Representative fluorescence images of healthy and AKI mice injected with DiD and DiD-labeled uEVs (DiD uEV), evaluated 4 h after EV injection. (B) Representative images of fluorescent dissected kidneys of AKI and healthy mice sacrificed 4 h after EV injection. Quantification of the fluorescence intensity of dissected kidneys treated with DiD uEVs, derived from healthy and AKI mice, was calculated in ROI (region of interest). Data are expressed as mean of average radiance ± SD (n = 6). Student's t test was performed: **$p < 0.001$, AKI versus healthy. (C) List of the 10 most expressed miRNAs in uEVs. (D) Histograms showing miRNA expression levels in renal tissue 4 h after vehicle or uEV injection. Data are normalized to RNU6B and to 1 for vehicle and expressed as mean ± SD of relative quantification (RQ) (n = 4/group). (E) Histograms showing the downregulation of selected miRNA targets (SMAD1, SMAD2, CCND1, and c-Myc), represented by relative quantification (RQ), in healthy and AKI mice, treated with saline (vehicle) and uEVs, respectively, at day 3 after damage. Data are normalized to GAPDH and to 1 for vehicle and are expressed as the mean ± SEM of healthy (n = 3), vehicle, and EVs (n = 7/group). One-way ANOVA was performed: *$p < 0.05$ versus vehicle.

miR-151 targets) were downregulated in the renal tissue of uEV-treated mice (Figure 4E).

uEVs Restore Klotho Levels in Injured Tissue

We then focused our attention on a specific renal factor, Klotho, involved in tissue regeneration. uEVs were found to contain Klotho, mainly the short soluble isoform (Figure 5A), at levels of 0.5–10 pg/2.0×10^8 EV particles, as determined by ELISA. In addition, Klotho mRNA was also detected within uEVs (32.05 ± 0.75 cycle threshold [Ct] value).

The expression of Klotho in renal tissue is known to decrease during acute and chronic damage.[40]

On the same line, in our data, renal tissue derived from AKI mice showed a significant reduction of Klotho at both mRNA and protein levels, compared with the tissue derived from healthy mice (Figures 5B–5E). Of interest, only uEV treatment, and not MSC EV treatment, significantly increased murine Klotho mRNA 4 h after injection (Figure 5B). However, no human Klotho mRNA was detected in injured renal tissue, excluding mRNA direct transfer. Moreover, the expression of Klotho protein, lost upon damage, was significantly restored to normal levels 4 and 48 h after uEV administration (Figures 5C and 5D).

The immunohistochemical analysis confirmed the restoration of Klotho levels, 48 h after EV injection, and showed the predominant localization of the protein to distal and proximal tubules (Figure 5E). We further analyzed the expression of two factors linked with the pro-regenerative effects of Klotho: CTGF[35,41] and α-SMA.[41] uEV treatment inhibited both CTGF and α-SMA upregulation observed in AKI mice (Figure 5F).

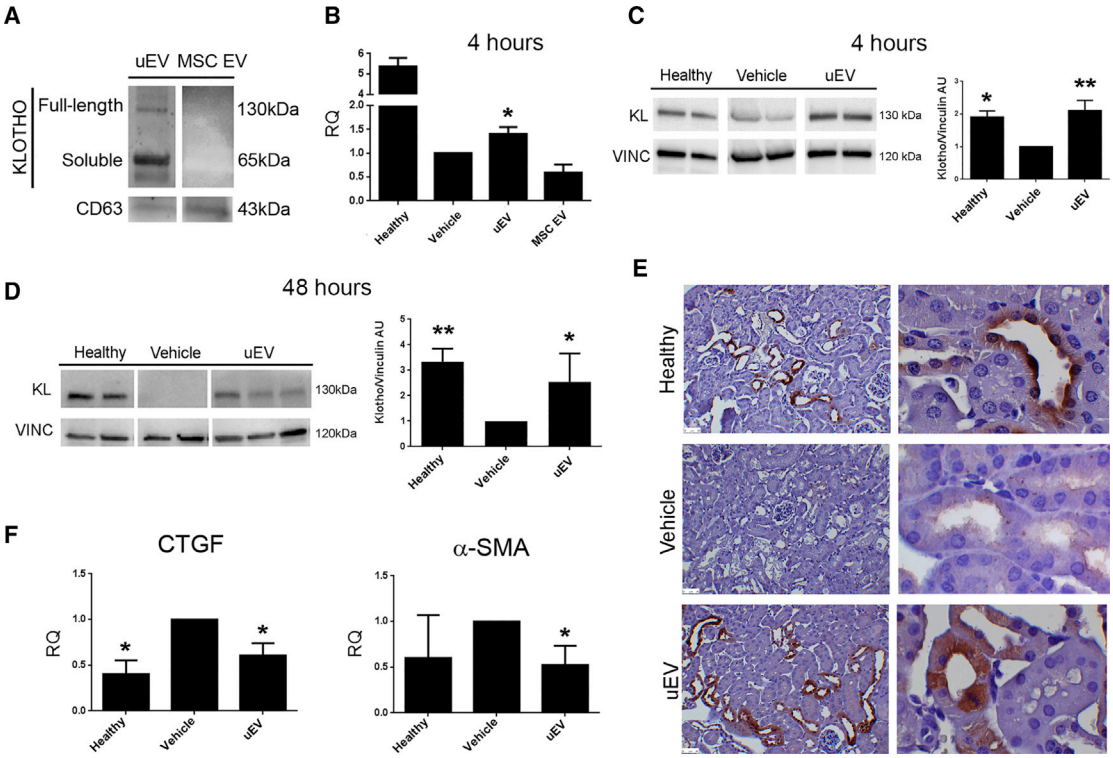

Figure 5. uEVs Restore Klotho Levels upon AKI

(A) Representative western blot showing the presence of Klotho in uEVs, but not in MSC EVs. CD63 was used as a control exosomal marker. (B) Histogram showing the renal mRNA expression of Klotho represented by relative quantification (RQ) in healthy and AKI mice, treated with saline (vehicle), uEVs, and MSC EVs, and analyzed 4 h post EV administration. Data are normalized to GAPDH and to 1 for vehicle, and are expressed as the mean ± SEM of healthy, vehicle, and EVs (n = 3/group). Student's t test was performed: *p < 0.05 versus vehicle. (C and D) Representative western blot of Klotho expression in kidney tissue from healthy and AKI mice, upon saline (vehicle) and uEV treatment, at days 1 (C) and 3 (D) after damage (4 and 48 h after EV injection, respectively). Data are expressed as the mean ± SD of the band intensity of n = 5 (healthy group) and n = 7 (vehicle and uEV groups), normalized to vinculin and to vehicle. One-way ANOVA was performed: *p < 0.05 versus vehicle. (E) Representative micrographs showing Klotho expression in kidney tissues of healthy and AKI mice injected with saline (vehicle) and uEVs, at day 3 after damage. Original magnification ×200 and ×1,000. (F) Histograms showing the mRNA levels of CTGF and α-SMA, represented by relative quantification (RQ) in healthy and AKI mice, treated with saline (vehicle) and uEVs. Data are normalized to GAPDH and to 1 for vehicle, and are expressed as the mean ± SEM of healthy (n = 3), vehicle, and EVs (n = 7/group). One-way ANOVA was performed: *p < 0.05 versus vehicle.

Klotho-Carrying EVs Favor Renal Regeneration

To sustain the role of Klotho present in uEVs and to assess whether the administration of Klotho carried by EVs may have an advantage over the use of the recombinant Klotho, we compared their effect on renal regeneration. Mice were treated with uEVs (containing Klotho at 1 pg/2.0 × 10^8 EV particles) or human recombinant Klotho at the same quantity (1 pg/mouse). The administration of recombinant Klotho alone, at variance with uEVs, did not exert any protective effect in damaged renal tissue, as evaluated by BUN, creatinine, and tissue histology (Figure 6).

We further confirmed the presence of Klotho in EVs released by human proximal tubular epithelial cells (HK2) (Figure S4). Tubular cells are considered the major source of EVs found in urine.[19,20] Of interest, when quantified by ELISA, the amount of Klotho present in HK2 EVs was at the same range as the one in uEVs (1–2 pg/2.0 × 10^8 EV particles). We then analyzed the effect of HK2 EVs in our AKI model. As expected, HK2-derived EVs displayed a beneficial effect comparable with uEVs (Figure 6).

Indispensable Role of Klotho in the Reno-Protective Effect of uEVs

To dissect the role of Klotho in the reno-protective effect of uEVs, we compared the regenerative effect of uEVs isolated from the urine of wild-type and Klotho null mice. Whereas the effect of wild-type murine uEVs (muEVs) was superimposable to human uEVs, no effect was observed using Klotho null muEVs (Figure 7). In particular, Klotho null murine uEVs were completely ineffective in restoring tissue morphology and renal function (Figure 7). Klotho expression in muEVs isolated from the urine of Klotho null mice was restored by engineering EVs with human recombinant Klotho. In order to associate the role of Klotho, present in human uEVs, with the regenerative effect of uEVs, we then treated AKI mice with Klotho engineered EVs, deriving from the urine of Klotho null mice. The number of particles

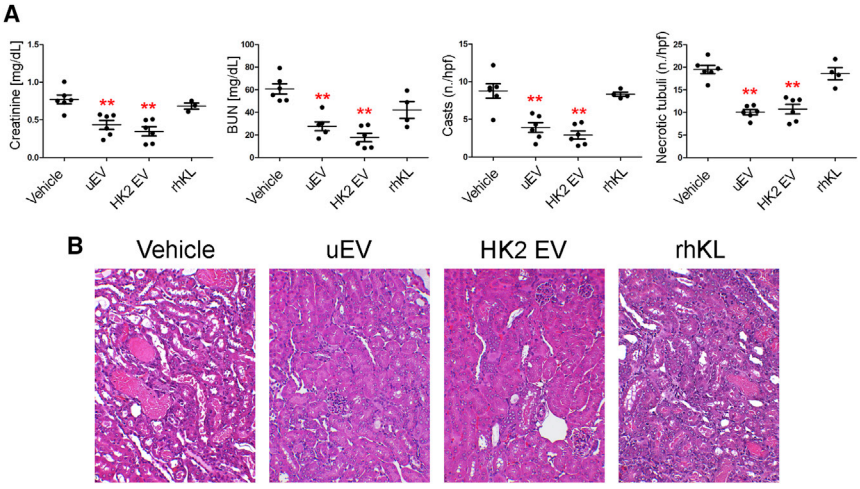

Figure 6. Effect of Klotho-Carrying EVs and Recombinant Klotho

(A) Creatinine and BUN levels and number of tubular hyaline casts and tubular necrosis in AKI mice treated with saline (vehicle), uEVs, HK2 EVs (n = 6), and recombinant Klotho (rhKL) (n = 4) at day 3 after damage. Data are expressed as mean ± SEM; ANOVA with Dunnett's multicomparison test was performed: *$p < 0.05$ or **$p < 0.001$ versus vehicle. (B) Representative micrographs of H&E of renal tissue from AKI mice treated with vehicle, uEVs, HK2 EVs, and recombinant Klotho (rhKL) at day 3 after damage. Original magnification ×200.

injected was determined based on the range of Klotho present in human μEVs (10 pg Klotho/mouse). The results showed that kidney damage was completely abrogated by the administration of Klotho engineered uEVs derived from Klotho null mice (Figure 7). Overall, our data suggest that Klotho present in human uEVs is responsible for promoting renal regeneration.

Regenerative Effect of Klotho Engineered EVs

To further extend the application of Klotho delivery via EVs for renal regeneration, we engineered ineffective fibroblast EVs with human recombinant Klotho (Figure S5). Klotho engineered fibroblast EVs promoted amelioration of renal function in AKI mice, reducing the levels of renal retention markers and tissue injury molecules (Figures 8A and 8B). In addition, histological evaluation of renal sections confirmed the beneficial effect of Klotho engineered fibroblast EVs on the maintenance of tissue architecture, with limited presence of casts and necrotic tubules in respect to fibroblast EV-treated mice (Figures 8C and 8D). In parallel, Klotho engineered fibroblast EVs significantly stimulated tubular cell proliferation (Figures 8C and 8D) and restored renal Klotho levels that were lost upon damage (Figures 8E and 8F). These results suggest a new potential strategy for renal tissue regeneration by engineering EVs with Klotho.

DISCUSSION

In our study, we evaluated the functional role of EVs obtained from urine of healthy subjects in renal regeneration, using an experimental murine model of AKI. Our results highlighted the beneficial effect of uEVs in AKI, an effect similar to that observed by MSC EVs. In particular, uEVs accelerated renal recovery, mitigating functional and histological abnormalities, characteristics of AKI, and stimulating tubular cell proliferation. Moreover, uEV treatment strongly abrogated the activation of several pro-inflammatory cytokines upon damage. Of interest, our study revealed the presence of the reno-protective factor Klotho within uEVs and the restoration of Klotho levels in injured tissue after uEV administration. Because EVs present in urine derive mainly from renal tubular cells, we further demonstrated the presence of Klotho in HK2 released EVs, as well as their beneficial effect in our AKI model. The role of Klotho within uEVs was dissected by engineering non-effective fibroblast EVs with human recombinant Klotho. Engineered fibroblast EVs, when administered in AKI mice, stimulated renal regeneration. Similarly, uEVs derived from Klotho null mice that did not exert any reno-protective effect acquired regenerative properties when engineered with human recombinant Klotho.

The pathogenesis of AKI is complex and involves tubular cell death, inflammation, and oxidative stress.[42] The use of stem cell-derived EVs, and in particular those released by MSCs, is considered a new innovative therapeutic strategy for renal regeneration.[43–46] However, the fact that MSC EVs are negative for Klotho suggests that MSC EVs and uEVs act through different renal regenerative mechanisms.

In our study, we suggest that EVs present in urine may be considered a new source of pro-regenerative EVs with a renal origin. Urinary EVs are considered to mainly derive from the epithelial cells along the nephron,[47–49] whereas EVs shed by cultured renal tubular cells have been described as effective in the recovery of ischemia reperfusion injury.[50] We here confirmed the renal origin and pro-regenerative properties of uEVs and by gradient density purification, we excluded the contribution of other non-vesicular contaminants in kidney repair.

The therapeutic properties of stem cell-derived EVs have been mainly attributed to their miRNA cargo.[9,51] In the current study, we demonstrated the preferential localization of labeled uEVs within injured kidneys, as well as the transfer of their specific miRNA cargo to damaged tissue. Interactome analysis of transferred uEV miRNA targets revealed several growth factor pathways, such as IGF-1 and HGF, previously implicated in the regenerative properties of MSC EVs.[9]

In addition, our study showed the specific presence of the renal factor Klotho in uEVs. Klotho, mainly produced in the kidney,[52] has been found to be involved in renal homeostasis/physiopathology, regulating transporter and ion channels.[53–55] The soluble form has been described to exert different anti-inflammatory, anti-apoptotic,

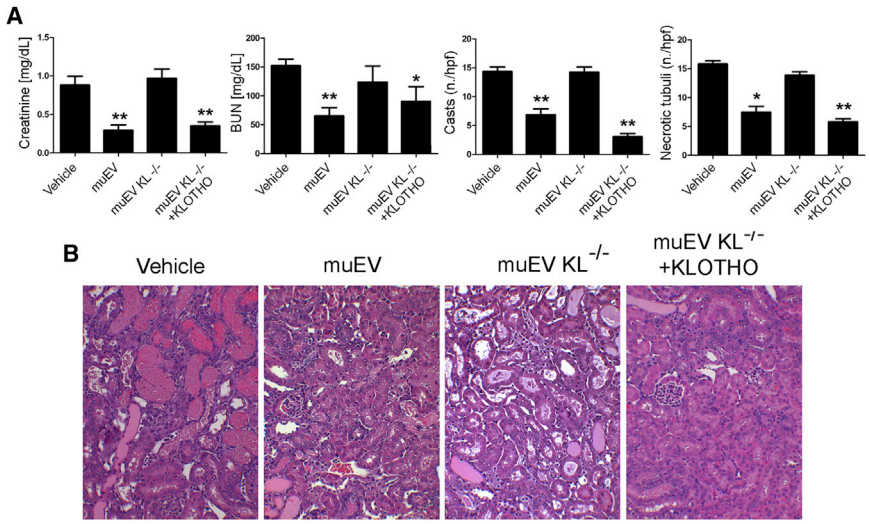

Figure 7. Regenerative Effect of Klotho-Engineered Murine uEVs

(A) Creatinine and BUN levels and number of tubular hyaline casts and tubular necrosis in AKI mice treated with vehicle, wild-type (muEV, 2.0 × 10^8/mouse), Klotho null murine uEVs (muEV $KL^{-/-}$, 2.0 × 10^8/mouse) (n = 6), and Klotho null murine uEVs engineered with human recombinant Klotho (muEV $KL^{-/-}$ + KLOTHO, 2.2 × 10^6/mouse) at day 3 after damage (n = 3). Data are expressed as mean ± SEM; ANOVA with Dunnett's multicomparison test was performed: *p < 0.05 or **p < 0.001 versus vehicle. (B) Representative micrographs of H&E of renal tissue from AKI mice treated with wild-type (muEV), Klotho null murine uEVs (muEV $KL^{-/-}$), and Klotho null murine uEVs engineered with human recombinant Klotho (muEV $KL^{-/-}$ + KLOTHO) at day 3 after damage. Original magnification ×200.

anti-oxidant, and anti-fibrotic effects in renal tissue.[53–59] Upon acute[31] and chronic damage,[32,33] Klotho levels have been shown to decline in blood, urine, and kidney. Administration of soluble Klotho, in preclinical models of AKI, is able to restore endogenous Klotho expression.[27,58–61] In addition, engineering of MSCs with Klotho resulted in an improvement of their regenerative capacity, increasing their anti-apoptotic and anti-fibrotic properties.[62,63]

Similarly, in our model, we found a strong reduction of Klotho expression in renal tissue of AKI mice, whereas uEV treatment promoted *de novo* Klotho synthesis, restoring normal Klotho levels. Moreover, miRNAs present in uEVs and transferred to the renal tissue may act synergistically on Klotho regulation. For instance, miR-30a, transferred by uEVs, has been described to be involved in Klotho upregulation by suppressing the methylation of the promoter.[64] In addition, CTGF and α-SMA, molecules involved in Klotho-related pathways,[27,35,41] were significantly downregulated by uEVs. miR-30a has also been shown to directly target CTGF in cultured cardiomyocytes and fibroblasts.[65] Moreover, miR-30 family and miR-151, transferred to renal tissue by uEV administration, resulted in the downregulation of SMAD1 and SMAD2, previously described to be implicated in the progression of kidney disease.[66] In addition, miR-151, a direct inhibitor of the mammalian target of rapamycin (mTOR) pathway, when transferred by MSC EVs, has been shown to ameliorate systemic sclerosis.[67]

The natural origin of EVs, along with their high stability in the circulation, makes them ideal candidates for targeted therapy by efficient transfer of molecules upon engineering.[68] The strategy of engineering EVs with pro-regenerative molecules is currently gaining an increasing interest.[69] However, the advantages in the use of EVs engineered with Klotho have not been reported yet. In the present study, Klotho was loaded onto fibroblast EVs, a Klotho negative EV source previously described as non-effective in renal repair,[70,71] and the inefficacy of naive EVs in AKI was reverted in parallel with the restoration of its endogenous levels. Moreover, the effect of recombinant Klotho administered alone at a dose comparable with that of uEVs (1 pg/mouse) did not exert any regenerative effect. This further underlines the ability of EVs as a delivery system, along with possible synergistic effects of the EV cargo.

To further confirm the role of Klotho, present in uEVs, and considering the limitations in obtaining human Klotho negative uEVs, we tested the efficacy of EVs isolated from urine of Klotho null mice, naive and following engineering with human Klotho. Interestingly, the lack of efficacy of Klotho null muEVs was reverted when engineered with human recombinant Klotho and injected at the same dose of Klotho present in human uEVs. This result suggested that the amount of Klotho carried by human uEVs is sufficient to exert its reno-protective effect.

In conclusion, in the present study, we propose an innovative use of uEVs as a therapeutic strategy for renal regeneration. uEVs from healthy subjects appear to be a novel source of vesicles with pro-regenerative properties displaying an effect on Klotho modulation. uEVs may facilitate intra-nephron communication by transferring regenerative mediators such as soluble Klotho.

MATERIALS AND METHODS

A detailed description of all methods used is provided in the Supplemental Materials and Methods.

Cell Culture

Human bone marrow MSCs were purchased from Lonza (Basel, Switzerland) and cultured in Mesenchymal Stem Cell Growth Medium (Lonza), as described previously.[8] MSCs were used up to the seventh passage of culture. Human lung fibroblast cells (line MRC5 PD19; Sigma-Aldrich, St. Louis, MO, USA) were cultured in DMEM (Lonza) plus 10% FCS (Lonza) and used up to passage 10. Human proximal tubular cells were purchased from ATCC

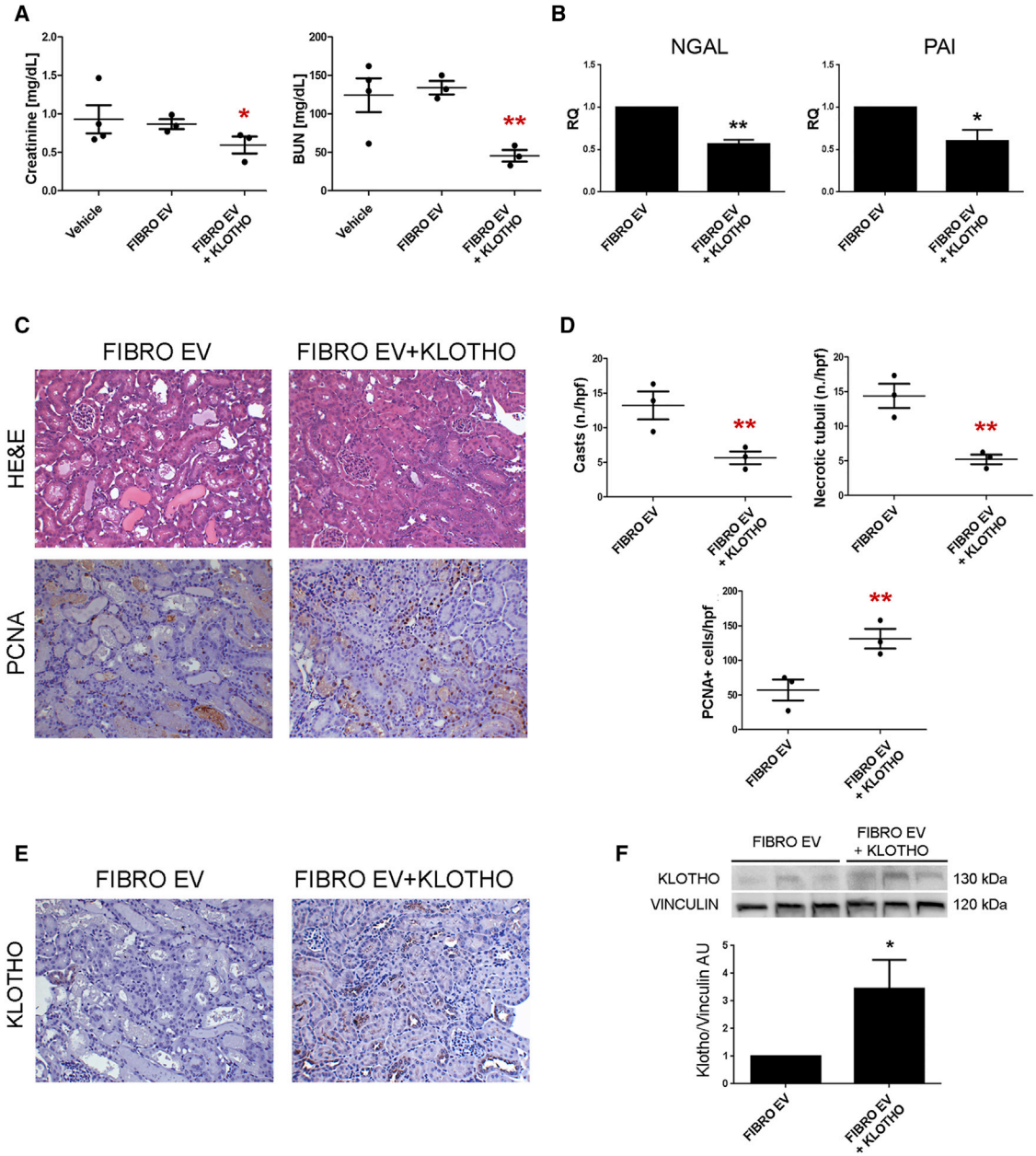

Figure 8. Regenerative Effect of Klotho-Engineered Fibroblast EVs

(A) Creatinine and BUN levels in AKI mice treated with FIBRO EVs and Klotho-engineered fibroblast EVs (FIBRO EV+KLOTHO) at day 3 after damage (n = 3). Data are expressed as mean ± SEM; ANOVA with Dunnett's multicomparison test was performed: *$p < 0.05$ or **$p < 0.001$ versus FIBRO EVs. (B) Histograms showing the renal mRNA expression represented by relative quantification (RQ) of NGAL and PAI in AKI mice treated with FIBRO EVs and Klotho-engineered fibroblast EVs (FIBRO EV+KLOTHO) (n = 3). Data are normalized to GAPDH and to 1 for vehicle and are expressed as the mean ± SEM; Student's t test was performed: *$p < 0.05$ or **$p < 0.001$ versus FIBRO EVs. (C) Representative micrographs of H&E and PCNA-positive staining of renal tissue from AKI mice treated with FIBRO EVs and Klotho-engineered fibroblast EVs (FIBRO EV+KLOTHO) at day 3 after damage. Original magnification ×200. (D) Quantification of tubular hyaline casts, tubular necrosis, and PCNA-positive cells at day 3 after damage (n = 3). Data are expressed as the mean ± SEM. Ten fields per section were analyzed. Student's t test was performed: **$p < 0.001$ versus FIBRO EVs. (E) Representative micrographs showing Klotho expression in kidney tissues of AKI mice treated with FIBRO EVs and Klotho-engineered fibroblast EVs (FIBRO EV+KLOTHO) at day 3 after damage. Original magnification ×200. (F) Western blot showing Klotho expression in injured kidney tissue treated with FIBRO EVs and Klotho-engineered fibroblast EVs (FIBRO EV+KLOTHO). Data are expressed as the mean ± SD of band intensity normalized to vinculin and to FIBRO EVs (n = 3). Student's t test was performed: *$p < 0.05$ versus FIBRO EVs.

(Manassas, VA, USA) and cultured in DMEM (Lonza) plus 10% FCS (Lonza).

Isolation of EVs

uEVs were isolated from the second morning urine (200 mL) of healthy volunteers (n = 14, female/male 1:1; age: 34 ± 5 years), as previously described.[72] Approval from the Review Board of A.O.U. Città della Salute e della Scienza hospital was obtained (Protocol number: 0021671). Consents from all subjects were obtained. The urine was first centrifuged at 3,000 rpm for 15 min to pellet cells and debris. Supernatant was collected and supplemented with protease inhibitor and NaN_3 10 mM (Sigma-Aldrich). After filtration through 0.8- and 0.45-μm filters (Merck Millipore, Billerica, MA, USA), samples were subdivided in 25-mL ultracentrifugation tubes and underwent ultracentrifugation (OPTIMA L-100 K Ultracentrifuge, Rotor Type 70-Ti; Beckman Coulter, Brea, CA, USA) at 100,000 × *g* for 1 h at 4°C. Pellets were further diluted in physiologic solution and underwent microfiltration with 0.22-μm and 2-h ultracentrifugation at 100,000 × *g* and 4°C. The pellet was then resuspended in DMEM (Lonza) + 1% DMSO (Sigma-Aldrich) and stored at −80°C. EV recovery was around 2–5 × 10^9 EVs/mL. Single uEV preparations were combined in pools (three donors per pool) that underwent a second ultracentrifugation in order to increase EV yield (n = 25 different pools). To increase the purity of uEVs, we applied a floating protocol through a sucrose gradient.[36] Five fractions were obtained and the highest one, containing pure EVs, was used.

Cell-derived EVs were obtained from MSC, HK2, and fibroblast supernatants, cultured overnight in RPMI deprived of FCS. Following the removal of cell debris and apoptotic bodies, by centrifugation at 3,000 × *g* for 15 min and microfiltration over a 0.22-μm filter, EVs were purified by 2-h ultracentrifugation at 100,000 × *g* and 4°C. EVs were resuspended in DMEM (Lonza) plus 1% DMSO (Sigma-Aldrich) and stored at −80°C.

For muEV isolation, urine obtained from 14 wild-type BALB/c and 13 $KL^{-/-}$ mice was collected in an Eppendorf tube twice a week over the course of approximately 8 weeks and stored at −80°C. muEVs were isolated using ExoQuick-TC (System Biosciences, Palo Alto, CA, USA), according to the manufacturer's protocol. muEVs were resuspended in DMEM (Lonza) plus 1% DMSO (Sigma-Aldrich) and stored at −80°C. Particle size and concentration were measured using NanoSight NS300 (NanoSight, Amesbury, UK) and analyzed using Nanoparticle Tracking Analysis software. EV recovery was around 1 × 10^9 EVs/mL.

For the engineering of EVs, human Klotho recombinant protein (R&D System, Minneapolis, MN, USA) was loaded onto EVs using the Exo-Fect Exosome Transfection Reagent (System Biosciences), according to the manufacturer's protocol.

EV Engineering

For the engineering of EVs, Klotho recombinant protein was loaded onto EVs using the Exo-Fect Exosome Transfection Reagent (System Biosciences), according to the manufacturer's protocol. In brief, 5 μg of EVs (quantified by Bradford) was incubated (by mixing) with 2.5 μg of recombinant Klotho in the presence of Exo-Fect solution for 1 h at +4°C. For the blockage of loading reaction, 30 μL of Exo-Quick-TC was added to the mixture and kept for 30 min on ice. A pellet of Klotho-loaded EVs was obtained by a further 10 min of centrifugation at 13,000 rpm.

Western Blot

Ten micrograms of EV-lysates and 50 μg of renal tissue lysates were loaded on Mini-PROTEAN TGX pre-cast electrophoresis gels (Bio-Rad, Hercules, CA, USA). Proteins were subsequently transferred on iBlot nitrocellulose membranes (Invitrogen, Carlsbad, CA, USA) and blotted with antibodies against Klotho (Abcam, Cambridge, UK), vinculin (Sigma-Aldrich), AQP1 (Santa Cruz Biotechnology, Dallas, TX, USA), AQP2 (Santa Cruz Biotechnology), CD63 (Santa Cruz Biotechnology), and calreticulin (Cell Signaling, Danvers, MA, USA). Chemiluminescent signal was detected using the ECL substrate (Bio-Rad).

Cytofluorimetric Analysis

Flow cytometric analysis was performed on EVs adsorbed onto surfactant-free white aldehyde/sulfate latex beads 4% w/v, 4-μm diameter (Molecular Probes, Carlsbad, CA, USA) using a FACSCalibur machine (Becton Dickinson, Franklin Lake, NJ, USA). The adsorbed EVs were analyzed with the following anti-human fluorescent-conjugated monoclonal antibodies: PDX-APC (allophycocyanin), CD24-fluorescein isothiocyanate (FITC), CD63-APC, VEGFR2-(VR2)-APC, CD81-phycoerythrin (PE), CD45-FITC, and CD42b-FITC. AQP1 and AQP2 were conjugated to an Alexa Fluor 488 dye through the Alexa Fluor Antibody Labeling Kit (Molecular Probes). Isotypic controls FITC-, PE-, or APC-conjugated Mouse IgG1 (all purchased by Miltenyi, Bergisch-Gladbach, Germany) were used.

Glycerol-Induced Model of AKI

Animal studies were conducted in accordance with the NIH *Guide for the Care and Use of Laboratory Animals* (Permit Number: 274/2015-PR). The *in vivo* experiments were conducted following the regulatory standards. As previously described,[8] AKI was performed in 8-week-old FVB mice by intramuscular injection of 8 mL/kg of 50% solution of hypertonic glycerol (Sigma) into inferior hindlimbs. On day 1 post injury, mice received a tail vein injection of 2.0 × 10^8 EVs in 100 μL saline or the same volume of saline (vehicle). The following EVs were tested: (1) uEVs isolated with ultracentrifuge; (2) uEVs isolated with floating protocol; (3) MSC EVs isolated with ultracentrifuge; and (4) EVs released by fibroblasts (n = 8 mice/group) and fibroblast EVs, engineered with human Klotho injected at the same particle number as uEVs (2.0 × 10^8 EVs/mouse) (n = 3). In addition, HK2 EVs (2.0 × 10^8 EVs/mouse) and recombinant Klotho (1 pg/mouse) (R&D Systems) were also tested (n = 6). Finally, muEVs (2.0 × 10^8 EVs/mouse), muEV $KL^{-/-}$ (2.0 × 10^8 EVs/mouse) (n = 6), and muEV $KL^{-/-}$ engineered with Klotho (n = 3), injected at the same amount of Klotho contained in human uEVs (10 pg/mouse; 2.2 × 10^6 EVs/mouse), were also used. Mice were sacrificed 48 h after the EV administration. A selected number of mice (n = 4/group) treated with uEVs, MSC EVs, and saline were sacrificed 4 h post

EV administration. After sacrifice, blood was recovered for evaluation of renal functional parameters, and kidneys were stored for histological and molecular analyses.

Molecular Analyses

uEV miRNA Content

Total RNA was extracted from a pool of uEVs deriving from 8 L of urine. uEVs were lysed in TRIzol (Ambion Waltham, MA, USA) and RNA was extracted using miRNeasy kit (QIAGEN, Hilden, Germany) following the manufacturer's protocol. Sixty nanograms of RNA was precipitated and pre-amplified prior to miRNA quantification. Expression of 380 different miRNAs was evaluated by quantitative real-time PCR using TaqMan Array MicroRNA card B (v.3.0) according to Megaplex protocol. Quantification was performed using a QuantStudio 12K Flex Real-Time PCR System (Applied Biosystems, Foster City, CA, USA). Ct values were analyzed by QuantStudio 12K Flex software (Applied Biosystems) using global normalization. miRNAs with raw Ct values higher than 35 were not included in the analysis.[14] For quantitative real-time PCR of uEV miRNAs, first-strand cDNA was produced from 200 ng of total RNA using the miScript Reverse Transcription kit (QIAGEN). miRNA expression analysis was performed using sequence-specific oligonucleotide primers (MWG-Biotech, Ebersberg, Germany) and the miScript SYBR Green PCR kit (QIAGEN). Relative quantification of the products was performed using a 96-well StepOne Real-Time System (Applied Biosystems).

Tissue mRNA Analysis

For the isolation of total RNA from mouse kidneys, pieces of around 50 mg of renal tissue were homogenized in 1 mL of TRIzol Reagent (Ambion) according to the manufacturer's protocol. First-strand cDNA was produced from 200 ng of total RNA using the High Capacity cDNA Reverse Transcription Kit (Applied Biosystems). For gene expression analysis, quantitative real-time PCR was performed, in a 20-μL reaction mixture containing 5 ng of cDNA template, the sequence-specific oligonucleotide primers (MWG-Biotech), and the Power SYBR Green PCR Master Mix (Applied Biosystems). mGAPDH was used as housekeeping normalizer. Fold change expression with respect to vehicle was calculated for all samples.

ELISA for Klotho

The quantification of Klotho levels within EVs was performed using an anti-human ELISA (Human soluble a-Klotho code 27998; Immuno-Biological Laboratories)[73] according to the manufacturer's protocol. In detail, three pools of uEVs, HK2 EVs, Klotho engineered fibroblast EVs, and muEV $KL^{-/-}$ engineered with Klotho were lysed in 40 μL of radioimmunopreciptation assay (RIPA) buffer and diluted (1:1 v/v) in the resuspension buffer provided in the ELISA.

Statistical Analysis

Results are generally expressed as mean ± SD or ± SEM, as indicated. Statistical analysis was performed by ANOVA with Dunnett's multicomparison test or by Student's t test when required. A p value <0.05 was considered significant.

SUPPLEMENTAL INFORMATION

Supplemental Information can be found online at https://doi.org/10.1016/j.ymthe.2019.11.013.

AUTHOR CONTRIBUTIONS

C.G.: EV engineering, *in vivo* studies, tissue analyses, and interpretation of results and manuscript writing. E.P.: EV isolation, western blot, RNA analysis, EV engineering, and interpretation of results and manuscript writing. V.D.: EV characterization and miRNA analyses. C.P. and J.M.: EV isolation and histological analyses. R.O. and L.J.N.: muEV collection. P.D.R.: study design, data interpretation, and manuscript writing. G.C.: electron microscopy analysis and manuscript writing. B.B.: study design and coordination, data interpretation, and manuscript writing.

CONFLICTS OF INTEREST

The authors declare no competing interests.

ACKNOWLEDGMENTS

We acknowledge funding from FP7 Marie Curie NephroTools ITN project and Miur ex60% (to B.B.) and NIH grant AG4059675 (to P.D.R.). We also acknowledge the technical support of Dr. Antico for histology and of Dr. Deregibus for electron microscopy.

REFERENCES

1. Morigi, M., Rota, C., and Remuzzi, G. (2016). Mesenchymal Stem Cells in Kidney Repair. Methods Mol. Biol. *1416*, 89–107.
2. Rewa, O., and Bagshaw, S.M. (2014). Acute kidney injury—epidemiology, outcomes and economics. Nat. Rev. Nephrol. *10*, 193–207.
3. Grange, C., Iampietro, C., and Bussolati, B. (2017). Stem cell extracellular vesicles and kidney injury. Stem Cell Investig. *4*, 90.
4. Pozzoli, S., Simonini, M., and Manunta, P. (2018). Predicting acute kidney injury: current status and future challenges. J. Nephrol. *31*, 209–223.
5. Zhao, L., Hu, C., Zhang, P., Jiang, H., and Chen, J. (2019). Genetic communication by extracellular vesicles is an important mechanism underlying stem cell-based therapy-mediated protection against acute kidney injury. Stem Cell Res. Ther. *10*, 119.
6. Bruno, S., Grange, C., Collino, F., Deregibus, M.C., Cantaluppi, V., Biancone, L., Tetta, C., and Camussi, G. (2012). Microvesicles derived from mesenchymal stem cells enhance survival in a lethal model of acute kidney injury. PLoS ONE *7*, e33115.
7. Gatti, S., Bruno, S., Deregibus, M.C., Sordi, A., Cantaluppi, V., Tetta, C., and Camussi, G. (2011). Microvesicles derived from human adult mesenchymal stem cells protect against ischaemia-reperfusion-induced acute and chronic kidney injury. Nephrol. Dial. Transplant. *26*, 1474–1483.
8. Bruno, S., Grange, C., Deregibus, M.C., Calogero, R.A., Saviozzi, S., Collino, F., Morando, L., Busca, A., Falda, M., Bussolati, B., et al. (2009). Mesenchymal stem cell-derived microvesicles protect against acute tubular injury. J. Am. Soc. Nephrol. *20*, 1053–1067.
9. Bruno, S., Tapparo, M., Collino, F., Chiabotto, G., Deregibus, M.C., Soares Lindoso, R., Neri, F., Kholia, S., Giunti, S., Wen, S., et al. (2017). Renal Regenerative Potential of Different Extracellular Vesicle Populations Derived from Bone Marrow Mesenchymal Stromal Cells. Tissue Eng. Part A *23*, 1262–1273.
10. Shen, B., Liu, J., Zhang, F., Wang, Y., Qin, Y., Zhou, Z., Qiu, J., and Fan, Y. (2016). CCR2 Positive Exosome Released by Mesenchymal Stem Cells Suppresses Macrophage Functions and Alleviates Ischemia/Reperfusion-Induced Renal Injury. Stem Cells Int. *2016*, 1240301.
11. Nassar, W., El-Ansary, M., Sabry, D., Mostafa, M.A., Fayad, T., Kotb, E., Temraz, M., Saad, A.N., Essa, W., and Adel, H. (2016). Umbilical cord mesenchymal stem cells

derived extracellular vesicles can safely ameliorate the progression of chronic kidney diseases. Biomater. Res. *20*, 21.

12. Tapparo, M., Bruno, S., Collino, F., Togliatto, G., Deregibus, M.C., Provero, P., Wen, S., Quesenberry, P.J., and Camussi, G. (2019). Renal Regenerative Potential of Extracellular Vesicles Derived from miRNA-Engineered Mesenchymal Stromal Cells. Int. J. Mol. Sci. *20*, E2381.
13. Tomasoni, S., Longaretti, L., Rota, C., Morigi, M., Conti, S., Gotti, E., Capelli, C., Introna, M., Remuzzi, G., and Benigni, A. (2013). Transfer of growth factor receptor mRNA via exosomes unravels the regenerative effect of mesenchymal stem cells. Stem Cells Dev. *22*, 772–780.
14. Collino, F., Bruno, S., Incarnato, D., Dettori, D., Neri, F., Provero, P., Pomatto, M., Oliviero, S., Tetta, C., Quesenberry, P.J., and Camussi, G. (2015). AKI recovery induced by mesenchymal stromal cell-derived extracellular vesicles carrying microRNAs. J. Am. Soc. Nephrol. *26*, 2349–2360.
15. Lai, R.C., Yeo, R.W., and Lim, S.K. (2015). Mesenchymal stem cell exosomes. Semin. Cell Dev. Biol. *40*, 82–88.
16. Ratajczak, J., Miekus, K., Kucia, M., Zhang, J., Reca, R., Dvorak, P., and Ratajczak, M.Z. (2006). Embryonic stem cell-derived microvesicles reprogram hematopoietic progenitors: evidence for horizontal transfer of mRNA and protein delivery. Leukemia *20*, 847–856.
17. Sallustio, F., Costantino, V., Cox, S.N., Loverre, A., Divella, C., Rizzi, M., and Schena, F.P. (2015). Retraction: Human renal stem/progenitor cells repair tubular epithelial cell injury through TLR2-driven inhibin-A and microvesicle-shuttled decorin. Kidney Int. *87*, 482.
18. Borges, F.T., Melo, S.A., Özdemir, B.C., Kato, N., Revuelta, I., Miller, C.A., Gattone, V.H., 2nd, LeBleu, V.S., and Kalluri, R. (2013). TGF-β1-containing exosomes from injured epithelial cells activate fibroblasts to initiate tissue regenerative responses and fibrosis. J. Am. Soc. Nephrol. *24*, 385–392.
19. Gildea, J.J., Seaton, J.E., Victor, K.G., Reyes, C.M., Bigler Wang, D., Pettigrew, A.C., Courtner, C.E., Shah, N., Tran, H.T., Van Sciver, R.E., et al. (2014). Exosomal transfer from human renal proximal tubule cells to distal tubule and collecting duct cells. Clin. Biochem. *47*, 89–94.
20. Street, J.M., Birkhoff, W., Menzies, R.I., Webb, D.J., Bailey, M.A., and Dear, J.W. (2011). Exosomal transmission of functional aquaporin 2 in kidney cortical collecting duct cells. J. Physiol. *589*, 6119–6127.
21. Pisitkun, T., Shen, R.F., and Knepper, M.A. (2004). Identification and proteomic profiling of exosomes in human urine. Proc. Natl. Acad. Sci. USA *101*, 13368–13373.
22. Gonzales, P.A., Pisitkun, T., Hoffert, J.D., Tchapyjnikov, D., Star, R.A., Kleta, R., Wang, N.S., and Knepper, M.A. (2009). Large-scale proteomics and phosphoproteomics of urinary exosomes. J. Am. Soc. Nephrol. *20*, 363–379.
23. Miranda, K.C., Bond, D.T., McKee, M., Skog, J., Păunescu, T.G., Da Silva, N., Brown, D., and Russo, L.M. (2010). Nucleic acids within urinary exosomes/microvesicles are potential biomarkers for renal disease. Kidney Int. *78*, 191–199.
24. Merchant, M.L., Rood, I.M., Deegens, J.K.J., and Klein, J.B. (2017). Isolation and characterization of urinary extracellular vesicles: implications for biomarker discovery. Nat. Rev. Nephrol. *13*, 731–749.
25. Hoorn, E.J., Pisitkun, T., Zietse, R., Gross, P., Frokiaer, J., Wang, N.S., Gonzales, P.A., Star, R.A., and Knepper, M.A. (2005). Prospects for urinary proteomics: exosomes as a source of urinary biomarkers. Nephrology (Carlton) *10*, 283–290.
26. Huang, J., Brenna, C., Khan, A.U.M., Daniele, C., Rudolf, R., Heuveline, V., and Gretz, N. (2019). A cationic near infrared fluorescent agent and ethyl-cinnamate tissue clearing protocol for vascular staining and imaging. Sci. Rep. *9*, 521.
27. Hu, M.C., Kuro-o, M., and Moe, O.W. (2013). Renal and extrarenal actions of Klotho. Semin. Nephrol. *33*, 118–129.
28. Kuro-o, M., Matsumura, Y., Aizawa, H., Kawaguchi, H., Suga, T., Utsugi, T., Ohyama, Y., Kurabayashi, M., Kaname, T., Kume, E., et al. (1997). Mutation of the mouse klotho gene leads to a syndrome resembling ageing. Nature *390*, 45–51.
29. Li, S.A., Watanabe, M., Yamada, H., Nagai, A., Kinuta, M., and Takei, K. (2004). Immunohistochemical localization of Klotho protein in brain, kidney, and reproductive organs of mice. Cell Struct. Funct. *29*, 91–99.
30. Hu, M.C., Kuro-o, M., and Moe, O.W. (2012). Secreted klotho and chronic kidney disease. Adv. Exp. Med. Biol. *728*, 126–157.
31. Panesso, M.C., Shi, M., Cho, H.J., Paek, J., Ye, J., Moe, O.W., and Hu, M.C. (2014). Klotho has dual protective effects on cisplatin-induced acute kidney injury. Kidney Int. *85*, 855–870.
32. Lu, X., and Hu, M.C. (2017). Klotho/FGF23 Axis in Chronic Kidney Disease and Cardiovascular Disease. Kidney Dis. (Basel) *3*, 15–23.
33. Sakan, H., Nakatani, K., Asai, O., Imura, A., Tanaka, T., Yoshimoto, S., Iwamoto, N., Kurumatani, N., Iwano, M., Nabeshima, Y., et al. (2014). Reduced renal α-Klotho expression in CKD patients and its effect on renal phosphate handling and vitamin D metabolism. PLoS ONE *9*, e86301.
34. Sugiura, H., Yoshida, T., Mitobe, M., Yoshida, S., Shiohira, S., Nitta, K., and Tsuchiya, K. (2010). Klotho reduces apoptosis in experimental ischaemic acute kidney injury via HSP-70. Nephrol. Dial. Transplant. *25*, 60–68.
35. Satoh, M., Nagasu, H., Morita, Y., Yamaguchi, T.P., Kanwar, Y.S., and Kashihara, N. (2012). Klotho protects against mouse renal fibrosis by inhibiting Wnt signaling. Am. J. Physiol. Renal Physiol. *303*, F1641–F1651.
36. Kowal, J., Arras, G., Colombo, M., Jouve, M., Morath, J.P., Primdal-Bengtson, B., Dingli, F., Loew, D., Tkach, M., and Théry, C. (2016). Proteomic comparison defines novel markers to characterize heterogeneous populations of extracellular vesicle subtypes. Proc. Natl. Acad. Sci. USA *113*, E968–E977.
37. Keller, S., Rupp, C., Stoeck, A., Runz, S., Fogel, M., Lugert, S., Hager, H.D., Abdel-Bakky, M.S., Gutwein, P., and Altevogt, P. (2007). CD24 is a marker of exosomes secreted into urine and amniotic fluid. Kidney Int. *72*, 1095–1102.
38. Cavallari, C., Ranghino, A., Tapparo, M., Cedrino, M., Figliolini, F., Grange, C., Giannachi, V., Garneri, P., Deregibus, M.C., Collino, F., et al. (2017). Serum-derived extracellular vesicles (EVs) impact on vascular remodeling and prevent muscle damage in acute hind limb ischemia. Sci. Rep. *7*, 8180.
39. Kumar, S., Liu, J., Pang, P., Krautzberger, A.M., Reginensi, A., Akiyama, H., Schedl, A., Humphreys, B.D., and McMahon, A.P. (2015). Sox9 Activation Highlights a Cellular Pathway of Renal Repair in the Acutely Injured Mammalian Kidney. Cell Rep. *12*, 1325–1338.
40. Hu, M.C., Kuro-o, M., and Moe, O.W. (2010). Klotho and kidney disease. J. Nephrol. *23* (*Suppl 16*), S136–S144.
41. Wu, Y.L., Xie, J., An, S.W., Oliver, N., Barrezueta, N.X., Lin, M.H., Birnbaumer, L., and Huang, C.L. (2017). Inhibition of TRPC6 channels ameliorates renal fibrosis and contributes to renal protection by soluble klotho. Kidney Int. *91*, 830–841.
42. Basile, D.P., Anderson, M.D., and Sutton, T.A. (2012). Pathophysiology of acute kidney injury. Compr. Physiol. *2*, 1303–1353.
43. Bruno, S., Porta, S., and Bussolati, B. (2016). Extracellular vesicles in renal tissue damage and regeneration. Eur. J. Pharmacol. *790*, 83–91.
44. Motavaf, M., Pakravan, K., Babashah, S., Malekvandfard, F., Masoumi, M., and Sadeghizadeh, M. (2016). Therapeutic application of mesenchymal stem cell-derived exosomes: A promising cell-free therapeutic strategy in regenerative medicine. Cell. Mol. Biol. *62*, 74–79.
45. Zhou, Y., Xu, H., Xu, W., Wang, B., Wu, H., Tao, Y., Zhang, B., Wang, M., Mao, F., Yan, Y., et al. (2013). Exosomes released by human umbilical cord mesenchymal stem cells protect against cisplatin-induced renal oxidative stress and apoptosis in vivo and in vitro. Stem Cell Res. Ther. *4*, 34.
46. Zou, X., Zhang, G., Cheng, Z., Yin, D., Du, T., Ju, G., Miao, S., Liu, G., Lu, M., and Zhu, Y. (2014). Microvesicles derived from human Wharton's Jelly mesenchymal stromal cells ameliorate renal ischemia-reperfusion injury in rats by suppressing CX3CL1. Stem Cell Res. Ther. *5*, 40.
47. Ranghino, A., Dimuccio, V., Papadimitriou, E., and Bussolati, B. (2015). Extracellular vesicles in the urine: markers and mediators of tissue damage and regeneration. Clin. Kidney J. *8*, 23–30.
48. Turco, A.E., Lam, W., Rule, A.D., Denic, A., Lieske, J.C., Miller, V.M., Larson, J.J., Kremers, W.K., and Jayachandran, M. (2016). Specific renal parenchymal-derived urinary extracellular vesicles identify age-associated structural changes in living donor kidneys. J. Extracell. Vesicles *5*, 29642.
49. Gracia, T., Wang, X., Su, Y., Norgett, E.E., Williams, T.L., Moreno, P., Micklem, G., and Karet Frankl, F.E. (2017). Urinary Exosomes Contain MicroRNAs Capable of Paracrine Modulation of Tubular Transporters in Kidney. Sci. Rep. *7*, 40601.

50. Dominguez, J.H., Liu, Y., Gao, H., Dominguez, J.M., 2nd, Xie, D., and Kelly, K.J. (2017). Renal Tubular Cell-Derived Extracellular Vesicles Accelerate the Recovery of Established Renal Ischemia Reperfusion Injury. J. Am. Soc. Nephrol. *28*, 3533–3544.

51. Gu, D., Zou, X., Ju, G., Zhang, G., Bao, E., and Zhu, Y. (2016). Mesenchymal Stromal Cells Derived Extracellular Vesicles Ameliorate Acute Renal Ischemia Reperfusion Injury by Inhibition of Mitochondrial Fission through miR-30. Stem Cells Int. *2016*, 2093940.

52. Kuro-o, M. (2010). Klotho. Pflugers Arch. *459*, 333–343.

53. Hu, M.C., Shi, M., Cho, H.J., Adams-Huet, B., Paek, J., Hill, K., Shelton, J., Amaral, A.P., Faul, C., Taniguchi, M., et al. (2015). Klotho and phosphate are modulators of pathologic uremic cardiac remodeling. J. Am. Soc. Nephrol. *26*, 1290–1302.

54. Kim, J.H., Xie, J., Hwang, K.H., Wu, Y.L., Oliver, N., Eom, M., Park, K.S., Barrezueta, N., Kong, I.D., Fracasso, R.P., et al. (2017). Klotho May Ameliorate Proteinuria by Targeting TRPC6 Channels in Podocytes. J. Am. Soc. Nephrol. *28*, 140–151.

55. Kuro-O, M. (2019). The Klotho proteins in health and disease. Nat. Rev. Nephrol. *15*, 27–44.

56. Sugiura, H., Yoshida, T., Tsuchiya, K., Mitobe, M., Nishimura, S., Shirota, S., Akiba, T., and Nihei, H. (2005). Klotho reduces apoptosis in experimental ischaemic acute renal failure. Nephrol. Dial. Transplant. *20*, 2636–2645.

57. Zhou, L., Li, Y., Zhou, D., Tan, R.J., and Liu, Y. (2013). Loss of Klotho contributes to kidney injury by derepression of Wnt/β-catenin signaling. J. Am. Soc. Nephrol. *24*, 771–785.

58. Hu, M.C., Shi, M., Gillings, N., Flores, B., Takahashi, M., Kuro-O, M., and Moe, O.W. (2017). Recombinant α-Klotho may be prophylactic and therapeutic for acute to chronic kidney disease progression and uremic cardiomyopathy. Kidney Int. *91*, 1104–1114.

59. Hu, M.C., Shi, M., Zhang, J., Quiñones, H., Kuro-o, M., and Moe, O.W. (2010). Klotho deficiency is an early biomarker of renal ischemia-reperfusion injury and its replacement is protective. Kidney Int. *78*, 1240–1251.

60. Chen, X., Tong, H., Chen, Y., Chen, C., Ye, J., Mo, Q., Zhao, G., Hong, G., Zheng, C., and Lu, Z. (2018). Klotho ameliorates sepsis-induced acute kidney injury but is irrelevant to autophagy. OncoTargets Ther. *11*, 867–881.

61. Hum, J.M., O'Bryan, L.M., Tatiparthi, A.K., Clinkenbeard, E.L., Ni, P., Cramer, M.S., Bhaskaran, M., Johnson, R.L., Wilson, J.M., Smith, R.C., and White, K.E. (2019). Sustained Klotho delivery reduces serum phosphate in a model of diabetic nephropathy. J. Appl. Physiol. (1985) *126*, 854–862.

62. Xie, L.B., Chen, X., Chen, B., Wang, X.D., Jiang, R., and Lu, Y.P. (2019). Protective effect of bone marrow mesenchymal stem cells modified with klotho on renal ischemia-reperfusion injury. Ren. Fail. *41*, 175–182.

63. Zhang, F., Wan, X., Cao, Y.Z., Sun, D., and Cao, C.C. (2018). Klotho gene-modified BMSCs showed elevated antifibrotic effects by inhibiting the Wnt/β-catenin pathway in kidneys after acute injury. Cell Biol. Int. *42*, 1670–1679.

64. Yin, S., Zhang, Q., Yang, J., Lin, W., Li, Y., Chen, F., and Cao, W. (2017). TGFβ-incurred epigenetic aberrations of miRNA and DNA methyltransferase suppress Klotho and potentiate renal fibrosis. Biochim. Biophys. Acta Mol. Cell. Res. *1864*, 1207–1216.

65. Duisters, R.F., Tijsen, A.J., Schroen, B., Leenders, J.J., Lentink, V., van der Made, I., Herias, V., van Leeuwen, R.E., Schellings, M.W., Barenbrug, P., et al. (2009). miR-133 and miR-30 regulate connective tissue growth factor: implications for a role of microRNAs in myocardial matrix remodeling. Circ. Res. *104*, 170–178, 6p, 178.

66. Lan, H.Y., and Chung, A.C. (2012). TGF-β/Smad signaling in kidney disease. Semin. Nephrol. *32*, 236–243.

67. Chen, C., Wang, D., Moshaverinia, A., Liu, D., Kou, X., Yu, W., Yang, R., Sun, L., and Shi, S. (2017). Mesenchymal stem cell transplantation in tight-skin mice identifies miR-151-5p as a therapeutic target for systemic sclerosis. Cell Res. *27*, 559–577.

68. Wiklander, O.P.B., Brennan, M.Á., Lötvall, J., Breakefield, X.O., and El Andaloussi, S. (2019). Advances in therapeutic applications of extracellular vesicles. Sci. Transl. Med. *11*, eaav8521.

69. de Jong, O.G., Kooijmans, S.A.A., Murphy, D.E., Jiang, L., Evers, M.J.W., Sluijter, J.P.G., Vader, P., and Schiffelers, R.M. (2019). Drug Delivery with Extracellular Vesicles: From Imagination to Innovation. Acc. Chem. Res. *52*, 1761–1770.

70. Kholia, S., Herrera Sanchez, M.B., Cedrino, M., Papadimitriou, E., Tapparo, M., Deregibus, M.C., Brizzi, M.F., Tetta, C., and Camussi, G. (2018). Human Liver Stem Cell-Derived Extracellular Vesicles Prevent Aristolochic Acid-Induced Kidney Fibrosis. Front. Immunol. *9*, 1639.

71. Grange, C., Tritta, S., Tapparo, M., Cedrino, M., Tetta, C., Camussi, G., and Brizzi, M.F. (2019). Stem cell-derived extracellular vesicles inhibit and revert fibrosis progression in a mouse model of diabetic nephropathy. Sci. Rep. *9*, 4468.

72. Dimuccio, V., Ranghino, A., Praticò Barbato, L., Fop, F., Biancone, L., Camussi, G., and Bussolati, B. (2014). Urinary CD133+ extracellular vesicles are decreased in kidney transplanted patients with slow graft function and vascular damage. PLoS ONE *9*, e104490.

73. Yamazaki, Y., Imura, A., Urakawa, I., Shimada, T., Murakami, J., Aono, Y., Hasegawa, H., Yamashita, T., Nakatani, K., Saito, Y., et al. (2010). Establishment of sandwich ELISA for soluble alpha-Klotho measurement: Age-dependent change of soluble alpha-Klotho levels in healthy subjects. Biochem. Biophys. Res. Commun. *398*, 513–518.

YMTHE, Volume *28*

Supplemental Information

Urinary Extracellular Vesicles Carrying Klotho Improve the Recovery of Renal Function in an Acute Tubular Injury Model

Cristina Grange, Elli Papadimitriou, Veronica Dimuccio, Cecilia Pastorino, Jordi Molina, Ryan O'Kelly, Laura J. Niedernhofer, Paul D. Robbins, Giovanni Camussi, and Benedetta Bussolati

Supplemental Methods

EV labelling

For biodistribution experiments uEVs were labelled during ultracentrifugation with liphofilic dye DiD fluorescent dye (TermoFisher Waltham. MA) as previously described.[1] One μM Vybrant Cell Tracers DiD was added during the ultracentrifugation procedure. Then, labelled uEVs were washed twice by ultracentrifugation in PBS (Lonza). Similar procedure was followed in the absence of uEV in order to collect potential dye aggregates to set the fluorescent background.

uEVs floating purification

To increase the purity of uEVs and separate vesicles from aggregates a floating protocol through a sucrose gradient was applied.[2] Briefly, ultracentrifuged EVs were resuspended in 1.35 ml of buffer (0.25 M sucrose, 10 mM Tris pH 8 and 1 mM EDTA, all products purchased by Sigma-Aldrich, St. Louis, MI), transferred to a SW55Ti rotor tube (Beckman Coulter) and mixed with 60% stock solution of Optiprep (Sigma-Aldrich) in a 1:1 ratio. Next, 1.2 ml of 20% Optiprep solution was layered on top, followed by 1.1 ml of 10% Optiprep solution. The tubes were then ultracentrifuged at 350.000 g for 1 hour at +4°C with “no brake” deceleration. The next day five fractions of 1 ml each were collected from the top of the tubes, each fraction was diluted in 25 ml PBS (Lonza) and ultracentrifuged at 100.000 g (rotor type 70Ti) for two hours at +4°C to pellet the EVs. The highest fraction, containing pure EVs, as assessed by NanoSight analysis, was then resuspended in 200 μl of DMEM (Lonza) plus 1% DMSO (Sigma-Aldrich) to allow freezing storage in -80°C until use.

EV quantification

EVs were analysed by nanoparticle tracking analysis (NTA) using the NanoSight NS300 system (NanoSight Ltd Salisbury, UK) configured with a Blue 488 nm laser and a high sensitivity digital camera system OrcaFlash 2.8. Hamamatsu C1 1440 (NanoSight Ltd). Briefly, EVs stored in -80°C were thawed, strongly vortexed and properly diluted in physiologic solution (Fresenius Kabi, Bad Homburg, Germany) previously filtered with 0.1 μm filter (Merck Millipore). For each sample, three videos of 30-second duration were recorded. The settings of acquisition and analysis were

optimized and kept constant between samples. The final analysis reported mean size and particles concentration.

Electron Microscopy

uEVs were loaded onto 200 mesh nickel formvar carbon coated grids (Electron Microscopy Science) for 20 min for transmission electron microscopy, followed by fixation in a 2.5% glutaraldehyde/2% sucrose solution. Samples were washed in distilled water, negatively stained with NanoVan (Nanoprobes, Yaphank) and examined by a Jeol JEM 1010 electron microscope (Joel, USA).

Cytofluorimetric analysis

As EVs are too small for FACScan analysis, analysis was performed on EVs bound to surfactant-free white aldehyde/sulfate latex beads 4% w/v 4 μm diameter (Molecular Probes, Invitrogen Carlsbad, CA). Five μl of beads were incubated with 30 μg of EVs for 30 min at room temperature and then for 30 min at +4°C.[3] Adsorbed EVs were divided in different vials and incubated with antibodies for 15 min at +4°C. The adsorbed EVs were then washed and analyzed with a FACSCalibur and CellQuest software (Becton Dickinson Bioscience Pharmingen. Franklyn Lake, NJ). Flow cytometry was performed using anti-human fluorescent-conjugated monoclonal antibodies (1:50 dilution): Podocalyxin-APC (PDX) (R&D, Minneapolis, #FAB1658A). CD24-FITC (Miltenyi, Bergisch Gladbach, Germany, #130-095-952). CD63-APC (Miltenyi, #130-100-173). VEGFR2-APC (VR2) (Miltenyi, #130-093-601). CD81-PE (Becton Dickinson, Franklin Lakes, New Jersey, #555676). CD45-FITC (Becton Dickinson, #555482) and CD42b-FITC (Becton Dickinson, #555472). Aquaporin-1 (AQP1) (Santa Cruz Biotechnology, Dallas, TX, #sc-20810) and Aquaporin-2 (AQP2) (Santa Cruz, #sc-28629) were conjugated to an Alexa Fluor® 488 dye through the Alexa Fuor® Antibody Labeling Kit (Molecular Probes. #A20181) following the manufacturer's instructions and used at 1:250 dilution. Gating was performed on the physical parameters dot plot. Controls were represented by EVs adsorbed on beads and marked with FITC-, PE- or APC- conjugated Mouse IgG1 Isotypes (all purchased by Miltenyi, #130-092-213, #130-

092-212 and #130-092-214). Beads with antibodies in the absence of EVs did not show positive fluorescence (not shown).

uEV miRNA content

Total RNA was extracted from a pool of uEVs deriving from 8 litres of urine. uEVs were lysed in Trizol (Ambion, Waltham, MA) and RNA extracted using miRNeasy kit (Qiagen Hilden, Germany) following the manufacturer's protocol. After isolation, total RNA concentration was evaluated using a ND-1000 spectrophotometer (Nanodrop ND-1000, Waltham, MA). Sixty nanograms of RNA were precipitated and pre-amplified prior to miRNA quantification. 380 different miRNAs expression was evaluated by quantitative real-time PCR (qRT-PCR) using Taqman Array MicroRNA card B (v3.0) according to Megaplex protocol. Quantification was performed using a QuantStudio 12K Flex Real-Time PCR System (Applied Biosystems, Foster City, CA). Cycle threshold (Ct) values were analysed by QuantStudio 12K Flex software (Applied Biosystems) using global normalization. MiRNAs with raw Ct values higher than 35 were not included in the analysis.

For qRT-PCR, RNA was purified from uEV using the *mirVana* miRNA Isolation Kit (Ambion) according to the manufacturer's protocol. First-strand cDNA was produced from 200 ng of total RNA using the miScript Reverse Trascription kit (Qiagen). MiRNA expression analysis was performed by qRT-PCR in 20 µl reaction mixture containing 4 ng of cDNA template, the sequence-specific oligonucleotide primers (purchased from MWG-Biotech, Ebersberg, Germany) and the miScript SYBR Green PCR kit (Qiagen). The snoRNA RNU6B was used as normalizer. Relative quantification of the products was performed using a 96-well StepOne Real-Time System (Applied Biosystems). miRNAs with raw *C*t values greater than 35 were not included in the analysis. Sequence specific oligonucleotide primers are reported below.

	Sequences
RNU6B	5′-CGCAAGGATGACACGCAA -3′
Mir-30a-3p	5′-CTTTCAGTCGGATGTTTGCAGC-3′
Mir-30e-3p	5′-CTTTCAGTCGGATGTTTACAGC-3′

Mir-30a-5p	5′-TGTAAACATCCTCGACTGGAA-3′
Mir-30d-3p	5′-CTTTCAGTCAGATGTTTGCTGC-3′
Mir-10b-3p	5′-ACAGATTCGATTCTAGGGGAAT-3′
Mir-664a-3p	5′-TATTCATTTATCCCCAGCCTACA-3′
Mir-151a-3p	5′-CTAGACTGAAGCTCCTTGAGG-3′
Mir-1260a	5′-ATCCCACCTCTGCCACCA-3′
Mir-31-3p	5′-TGCTATGCCAACATATTGCCAT-3′
Mir-151a-5p	5′-TCGAGGAGCTCACAGTCTAGT-3′

Funrich analysis tool was used to perform target prediction analysis.[4] Network analysis to define the associated pathways of the predictive genes was generated by the FunRich interaction plug-in (p-value <0.01 in the enriched pathways). A filter of a minimum of six interactions among different nodes was applied.

Blood analysis for renal function

Blood samples for the quantification of serum creatinine and BUN were performed using a colorimetric microplate assays (Quantichrom Creatinine Assay, BioAssay Systems and Quantichrom Urea Assay, BioAssay Systems, Hayward, CA) following the manufacturer's guidelines. Creatinine kinase activity was also quantified using the Cobas e 411 analyser (Roche, Basel, Switzerland), as previously described.[5]

Morphological Studies

For renal histology, 5 μm thick paraffin kidney sections were routinely stained with haematoxylin and eosin (Merck Millipore). Luminal hyaline casts and tubular necrosis (denudation of tubular basement membrane) were assessed in non-overlapping fields (up to 10 for each section) using a 20× objective (high power field, HPF).[4] Number of casts and tubular profiles showing necrosis was recorded in a single blind fashion. The presence of ferric iron within renal tissue was evaluated using "PEARLS for ferric iron" staining (Bi-Optica, Milano, IT) following the manufacture's protocol.

Immunohistochemistry for the detection of proliferation of tubular cells was performed. Kidney sections of paraffin-embedded samples were stained with a monoclonal anti-PCNA antibody (Proliferating Cell Nuclear Antigen) (Santa Cruz). Apoptosis was evaluated using the TUNEL assay analysis (ApopTagOncor, Gaithersburg, MD), following the manufacture's protocol. Number of PCNA-positive cells and of TUNEL-positive nuclei was evaluated by counting the number of positive nuclei per field in 10 randomly chosen sections of kidney cortex (20× magnification) using ImageJ software. Immunohistochemistry for the detection of Klotho was performed using a polyclonal anti-Klotho antibody (Abcam, Cambridge, UK). Immunoperoxidase reactions were performed using anti-rabbit HRP antibody (Pierce, Rockford, IL).

Optical imaging and biodistribution of uEVs

Nude mice were used to evaluate the accumulation of labelled uEVs within injured kidneys. Healthy and AKI mice were intravenously injected with $1.5x10^{10}$ DiD-labeled uEVs (n=6). Three healthy mice and 3 AKI mice received DID dye (Molecular Probes, Invitrogen) alone in order to set fluorescence background measurement. All studies were performed with IVIS 200 small animal imaging system (PerkinElmer. Waltham. MA) using excitation filter at 640 nm and emission filter at 700 nm. Fluorescence emission was normalized to photons per second per centimetre squared per steradian (p/sec/cm^2/sr). Mice were anesthetized with 2.5% isoflurane (Merial, Lyon, France) and images were acquired in the prone position after four hours post EV injection. Then, mice were sacrificed and dissected kidneys were imaged immediately as previously described.[1] The fluorescence signal was quantified in the kidney region in ROI draw freehand. The relative mean fluorescence intensity of each ROI was obtained by subtracting the mean fluorescence intensity of the corresponding ROI of the fluorescence intensity of mice treated with DiD alone. Data were expressed as the average radiance ±SD. Images were acquired and analysed using Living Image 4.0 software (Perkin Elmer).

Tissue RNA isolation – Real Time PCR

For the isolation of RNA from mouse kidneys, pieces of around 50 mg of renal tissue were homogenized in 1 ml of Trizol Reagent (Ambion) according to the manufacturer's protocol. RNA was then quantified spectrophotometrically by Nanodrop. First-strand cDNA was produced from 200 ng of total RNA using the High Capacity cDNA Reverse Transcription Kit (Applied Biosystems). For gene expression analysis, qRT-PCR was performed in 20 μl reaction mixture containing 5 ng of cDNA template, the sequence-specific oligonucleotide primers (purchased from MWG-Biotech) and the Power SYBR Green PCR Master Mix (Applied Biosystems). mGAPDH was used as housekeeping normalizer. Fold change expression respect to 1 for Vehicle was calculated for all samples. The sequence-specific oligonucleotide primers used are shown in the following table.

	Forward	Reverse
mGAPDH	5′-AACTTTGGCATTGTGGAAGG-3′	5′-ACACATTGGGGGTAGGAACA-3′
mNGAL	5′-TGCACAGGTATCCTCAGGTACAGA-3′	5′-GGAAAAATACCATGGCGAACTG-3′
mPAI	5′-AGTCAATGAGAAGGGCACAGCT-3′	5′-TAGGTCCCGCTGGACAAAGAT-3′
mSOX9	5′-AGTACCCGCATCTGCACAAC-3′	5′-ACGAAGGGTCTCTTCTCGCT-3′
mCASP3	5′-CCATAAGAGCACTGGAATGTCATC-3′	5′-TCCAAAATGTCTTCACGAGTAAGATC-3′
mASMA	5′-GAGGCACCACTGAACCCTAA-3′	5′-CATCTCCAGAGTCCAGCACA-3′
mSMAD1	5′-TTCAGATGCCAGCTGACACAC-3′	5′-CCTCTGCTGATTTCAGCGG -3′
mSMAD2	5′-TGAGACCCCAGTCTTGCCTC-3′	5′-CTGTGGCTCAATTCCTGCTG-3′
mc-Myc	5′-ACCAGCAGCGACTCTGAAGAAG-3′	5′-ATGGAGATGAGCCCGACTCC-3′
mCCND1	5′-CCTGGATGCTGGAGGTCTGT-3′	5′-CCAGGGACAGGAAGCGGT-3′
mCTGF	5′-CTTCTGCGATTTCGGCTCC-3′	5′-TGCTTTGGAAGGACTCACCG-3′
mTNF-a	5′-CATCTTCTCAAAATTCGAGTGACAA-3′	5′-TGGGAGTAGACAAGGTACAACCC-3′
mNF-kB	5′-ACAGGTCAAAATTTGCAACTATGTG-3′	5′-TGCATACCCCGTCCTCACA-3′
mIL1-beta	5′-CAACCAACAAGTGATATTCTCCATG-3′	5′-GATCCACACTCTCCAGCTGCA-3′
mIL6	5′-ACCAGAGGAAATTTTCAATAGGC-3′	5′-TGATGCACTTGCAGAAAACA-3′
h-KLOTHO	5′-GGAAACCTTAAAAGCCATCAAGCT-3′	5′-GAAGACTTTGGCAACAACATC TTG T-3′

miRNA transfer in renal tissue

miRNA transfer in renal tissue was evaluated by qRT-PCR using the miScript SYBR Green PCR kit (Qiagen). The snoRNA RNU6B was used as normalizer. Relative quantification of the products

was performed using a 96-well StepOne Real-Time System (Applied Biosystems). Fold change expression in respect to Vehicle was calculated for all samples. The sequence-specific oligonucleotide primers used are shown in table in “uEV miRNA content” section.

Western Blot

For protein analysis of renal tissue, pieces of around 50 mg were homogenized in 1 ml of RIPA buffer, containing 1% of Phosphatase Inhibitor Cocktails. Protease Inhibitors and PMSF (all products purchased by Sigma-Aldrich). Proteins from EVs were extracted using the same lysis buffer, while protein concentration was estimated by Bradford (Bio-Rad, Hercules, CA) quantification. Ten μg of EV-lysates and 50 μg of renal tissue lysates were loaded on Mini-PROTEAN TGX pre-cast electrophoresis gels (Bio-Rad). Proteins were subsequently transferred on iBlot nitrocellulose membranes (Invitrogen) and blotted with antibodies against Klotho (Abcam. #181373), Vinculin (Sigma-Aldrich, #V4505), AQP1 (Santa Cruz Biotechnology, sc-20810), AQP2 (Santa Cruz Biotechnology, sc-28629), CD63 (Santa Cruz Biotechnology, sc-15363) and Calreticulin (Cell Signaling, Danvers, Massachusetts, #2891). Chemiluminescent signal was detected using the ECL substrate (Bio-Rad).

Supplemental References:

1. Grange C. Tapparo M. Bruno S. Chatterjee D. Quesenberry PJ. Tetta C. et al.: Biodistribution of mesenchymal stem cell-derived extracellular vesicles in a model of acute kidney injury monitored by optical imaging. Int J Mol Med 33: 1055-1063. 2014.
2. Kowal J. Arras G. Colombo M. Jouve M. Morath JP. Primdal-Bengtson B. et al.: Proteomic comparison defines novel markers to characterize heterogeneous populations of extracellular vesicle subtypes. Proc Natl Acad Sci USA 113: E968–977. 2016.
3. Dimuccio V. Ranghino A. Praticò Barbato L. Fop F. Biancone L. Camussi G. et al.: Urinary CD133+ extracellular vesicles are decreased in kidney transplanted patients with slow graft function and vascular damage. PLoS One 9(8): e104490. 2014.
4. Bruno S. Tapparo M. Collino F. Chiabotto G. Deregibus MC. Soares Lindoso R. et al.: Renal Regenerative Potential of Different Extracellular Vesicle Populations Derived from Bone Marrow Mesenchymal Stromal Cells. Tissue Eng Part A 23: 1262-1273. 2017.
5. Moggio A. Geraci S. Boido A. Sticht C. Gretz N. Bussolati B: Assessment of an acute kidney injury in rhabdomyolytic mice by transcutaneous measurement of sinistrin excretion. Nephrol Dial Transplant 1;32(7):1167-1175. 2017.

Supplemental Figures

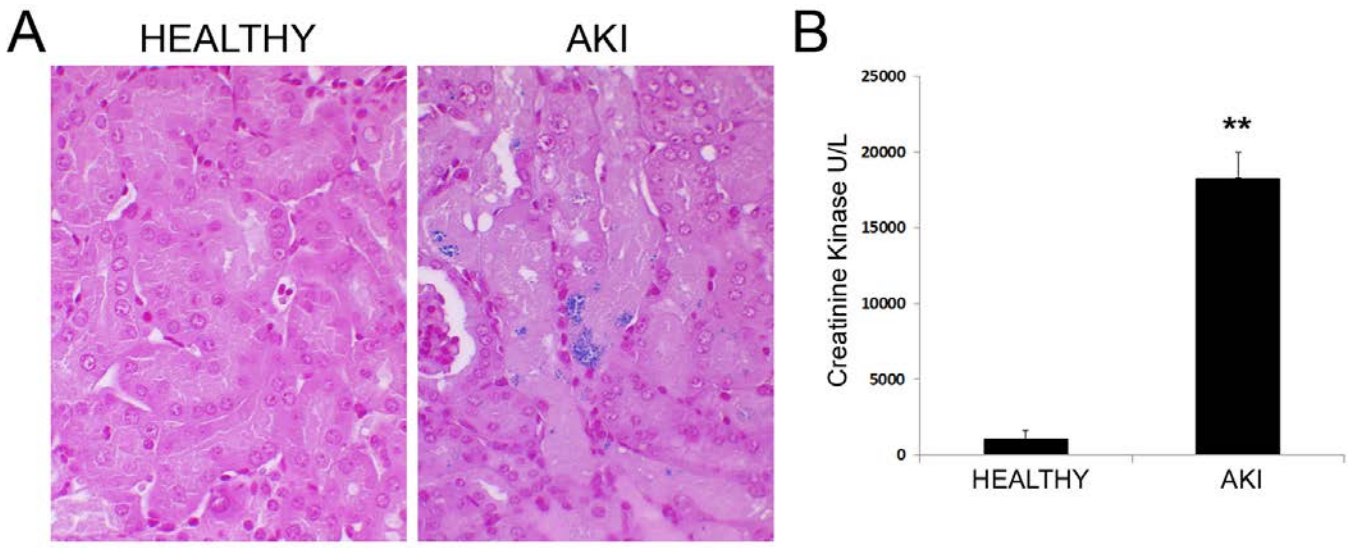

Supplemental Figure 1. Assessment of glycerol induced rhabdomyolysis. (A) Representative images of Pearls staining showing iron deposits (in blue) on renal tissue of Healthy and AKI mice. Original magnification: x200. (B) Histograms representing the level of the muscle damage marker creatinine kinase (U/L) in Healthy and AKI mice, 24 hours post glycerol injection (n=3).

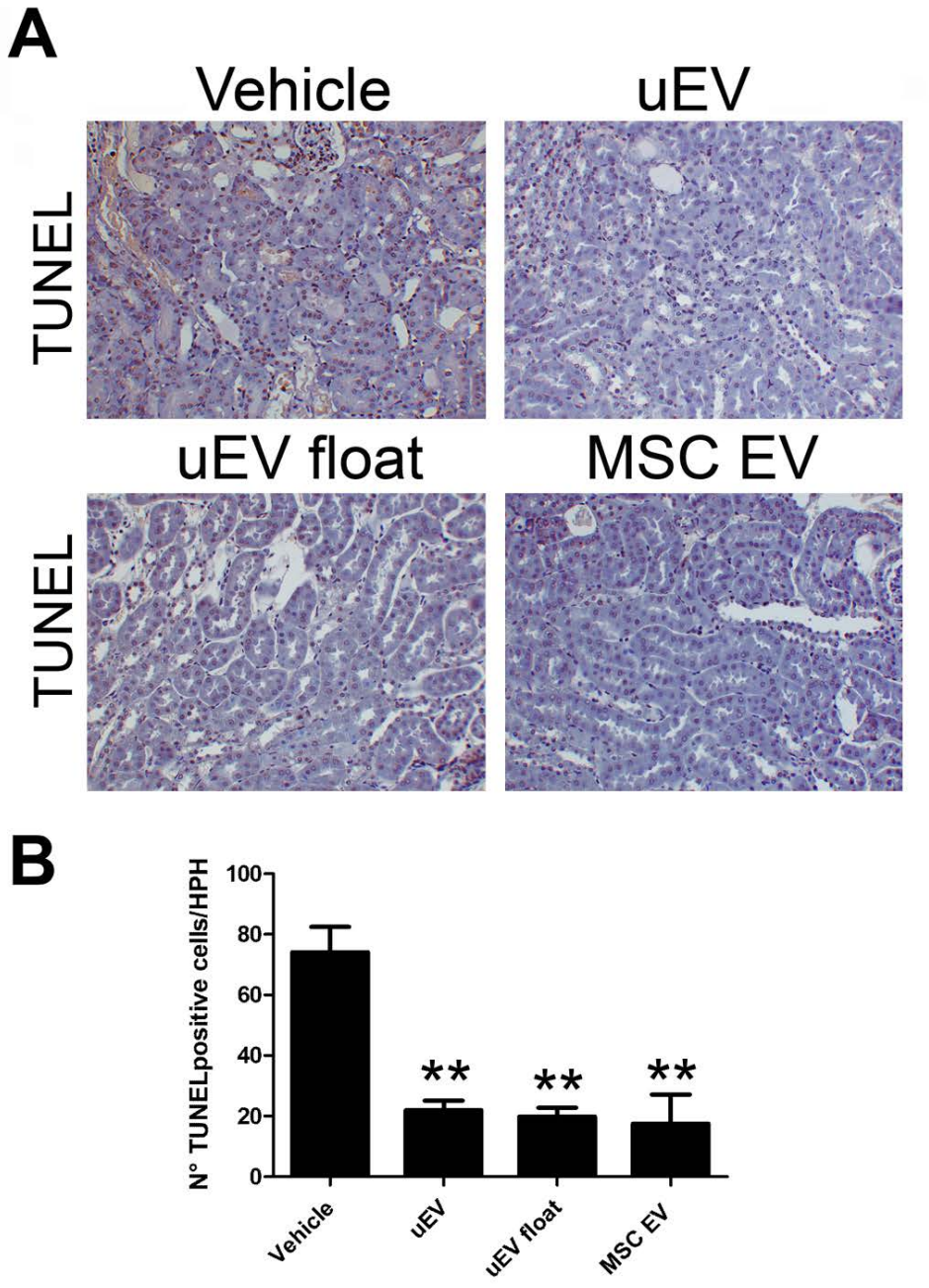

Supplemental Figure 2. uEVs abrogate tubular cell apoptosis. (A) Representative micrographs showing TUNEL positive cells in kidney tissues from AKI mice injected with saline (Vehicle), uEVs, uEVs float and MSC EVs, at day 3 after damage. Original magnification: x200. (B) Quantification of TUNEL positive cells in AKI mice treated or not (Vehicle) with EVs at day 3 post damage. Data are expressed as the mean ±SEM of the count of 10 fields/section (n=4 mice for each group). ANOVA with Dunnet's multicomparison test was performed: **p<0.001 versus Vehicle.

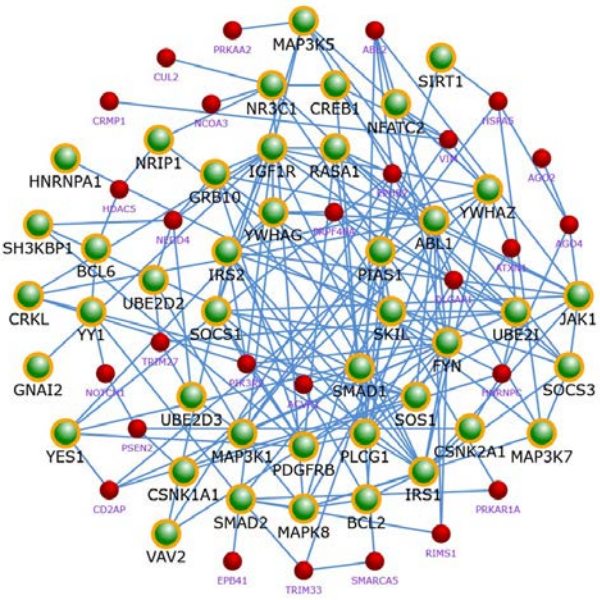

Supplemental Figure 3. Network interactome analysis. Network interactome analysis of the uEVs predictive genes targeted by the four transferred miRNAs. The yellow node boundary represents the selected candidate molecules associated with the following highly over-represented pro regenerative pathways: proteoglycan–syndecan signalling events, IGF-1 and HGF ($p<0.001$).

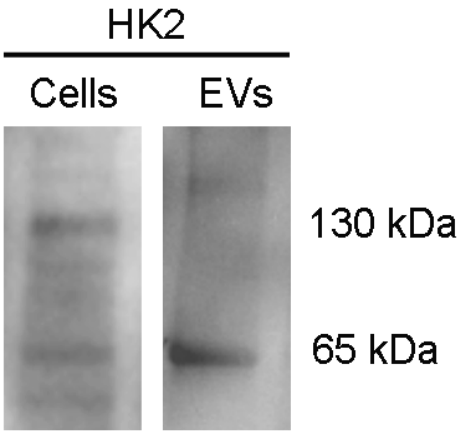

Supplemental Figure 4. Klotho expression in HK2 cells and derived EVs. Representative Western blot showing the presence of Klotho in HK2 cells and isolated EVs.

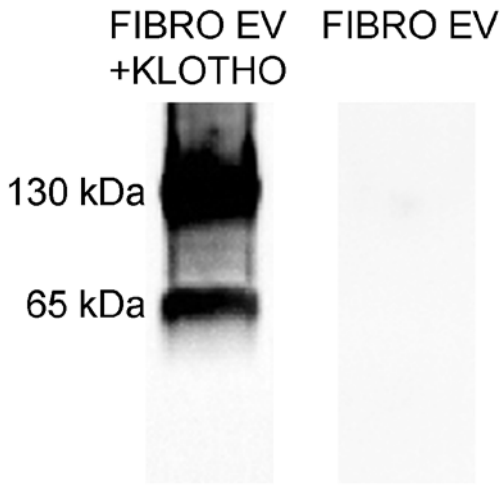

Supplemental Figure 5. Engineering of fibroblast derived EVs with human recombinant Klotho. Representative western blot showing the efficient engineering of FIBRO EVs with human recombinant Klotho, absent in native FIBRO EVs.

Supplemental Table 1. miRNAs expressed by uEVs by Array. MicroRNAs expressed by uEVs listed in the order of expression level.

miRNAs expressed by uEVs			
miRNAs	Average CT value	miRNAs	Average CT value
hsa-miR-30a-3p	16.121	hsa-miR-935	30.147
hsa-miR-30e-3p	16.845	hsa-miR-1247-5p	30.366
hsa-miR-30a-5p	17.253	hsa-miR-20b-3p	30.374
hsa-miR-30d-3p	19.445	hsa-miR-148a-5p	30.393
hsa-miR-10b-3p	19.578	hsa-miR-136-3p	30.412
hsa-miR-664a-3p	19.732	hsa-miR-1251-5p	30.419
hsa-miR-151a-3p	20.843	hsa-miR-92a-1-5p	30.468
hsa-miR-1260a	21.445	hsa-miR-944	30.468
hsa-miR-31-3p	22.564	hsa-miR-765	30.483
hsa-miR-151a-5p	22.980	hsa-miR-190b	30.519
hsa-miR-7-1-3p	23.192	hsa-miR-483-3p	30.738
hsa-miR-29c-5p	23.716	hsa-miR-141-5p	30.889
hsa-miR-200a-5p	23.800	hsa-miR-129-1-3p	30.952
hsa-miR-766-3p	23.857	hsa-miR-18a-3p	31.169
hsa-miR-625-3p	23.866	hsa-miR-1303	31.231
hsa-miR-93-3p	24.284	hsa-miR-892b	31.314
hsa-miR-378a-3p	24.363	hsa-miR-378a-5p	31.321
hsa-miR-1180-3p	24.505	hsa-miR-638	31.361
hsa-miR-181a-2-3p	24.667	hsa-miR-24-2-5p	31.365
hsa-miR-99b-3p	24.747	hsa-let-7c-3p	31.371
hsa-miR-425-3p	24.753	hsa-miR-1236-3p	31.387
hsa-miR-183-3p	24.832	hsa-miR-939-5p	31.397
hsa-miR-222-5p	24.846	hsa-miR-1296-5p	31.401
hsa-miR-577	24.853	hsa-miR-616-5p	31.466
hsa-miR-34a-3p	24.985	hsa-miR-1208	31.559
hsa-miR-1226-5p	2.5068	hsa-miR-33a-3p	31.612
hsa-miR-628-3p	25.087	hsa-miR-15a-3p	31.642
hsa-miR-26a-1-3p	25.093	hsa-miR-550a-3p	31.659
hsa-miR-590-3p	25.159	hsa-miR-196a-3p	31.736
hsa-miR-26b-3p	25.165	hsa-miR-1249-3p	31.891
hsa-miR-1271-5p	25.172	hsa-let-7a-3p	31.928
hsa-miR-335-3p	25.251	hsa-let-7f-2-3p	31.954
hsa-miR-409-3p	25.292	hsa-miR-144-3p	31.997
hsa-miR-629-3p	25.364	hsa-miR-125b-1-3p	32.005
hsa-miR-22-5p	25.389	hsa-miR-223-5p	32.047
hsa-miR-99a-3p	25.509	hsa-miR-520c-3p	32.065
hsa-miR-27a-5p	25.517	hsa-let-7i-3p	32.087
hsa-let-7d-3p	25.549	hsa-miR-1224-3p	32.103
hsa-miR-34b-3p	2.5629	hsa-miR-1244	32.116
hsa-miR-650	25.660	hsa-miR-24-1-5p	32.144
hsa-miR-27b-5p	25.802	hsa-let-7e-3p	32.165
hsa-miR-125b-2-3p	26.101	hsa-miR-1183	32.235
hsa-miR-9-3p	26.103	hsa-miR-144-5p	32.292
hsa-miR-20a-3p	26.144	hsa-miR-938	32.321
hsa-miR-130b-5p	26.316	hsa-miR-875-5p	32.352

hsa-miR-424-3p	26.336	hsa-let-7g-3p	32.359
hsa-miR-340-3p	26.355	hsa-miR-543	3.2391
hsa-miR-505-5p	26.465	hsa-miR-1276	32.449
hsa-miR-10a-3p	26.473	hsa-miR-200c-5p	32.474
hsa-miR-1275	26.513	hsa-miR-663b	32.547
hsa-miR-206	26.570	hsa-miR-221-5p	32.591
hsa-miR-1290	26.587	hsa-miR-769-3p	32.638
hsa-miR-769-5p	26.659	hsa-miR-639	32.683
hsa-miR-320b	26.698	hsa-miR-16-1-3p	32.775
hsa-miR-193b-5p	2.6713	hsa-miR-520d-3p	32.780
hsa-miR-1270	27.018	hsa-miR-1179	32.816
hsa-miR-589-3p	27.069	hsa-miR-374a-3p	32.825
hsa-miR-584-5p	27.179	hsa-miR-596	32.827
hsa-miR-942-5p	27.352	hsa-miR-100-3p	32.873
hsa-miR-148b-5p	27.529	hsa-miR-545-5p	32.982
hsa-miR-1233-3p	27.553	hsa-miR-1292-5p	32.992
hsa-miR-500a-3p	27.555	hsa-miR-92b-5p	33.104
hsa-miR-192-3p	27.563	hsa-miR-1301-3p	33.111
hsa-miR-454-5p	27.671	hsa-miR-550a-5p	33.178
hsa-miR-181c-3p	27.768	hsa-miR-581	33.179
hsa-miR-30d-5p	27.813	hsa-miR-572	33.187
hsa-miR-432-5p	27.889	hsa-miR-7-5p	33.283
hsa-miR-19b-1-5p	28.001	hsa-miR-770-5p	33.303
hsa-miR-29a-5p	28.013	hsa-miR-101-5p	33.351
hsa-miR-934	28.069	hsa-miR-1225-3p	33.448
hsa-miR-1269a	28.179	hsa-miR-1262	33.521
hsa-miR-191-3p	28.207	hsa-miR-661	33.591
hsa-miR-15b-3p	28.208	hsa-miR-34b-5p	33.598
hsa-miR-571	28.214	hsa-miR-548i	33.599
hsa-miR-622	28.297	hsa-miR-497-5p	33.654
hsa-miR-361-3p	28.301	hsa-miR-1305	33.756
hsa-miR-30c-2-3p	28.364	hsa-miR-1267	33.822
hsa-miR-135b-3p	28.381	hsa-miR-943	33.830
hsa-miR-194-3p	28.409	hsa-miR-302d-5p	33.913
hsa-miR-941	28.549	hsa-miR-513c-5p	33.968
hsa-miR-200b-5p	28.778	hsa-miR-1265	34.069
hsa-miR-592	28.893	hsa-miR-23b-5p	34.075
hsa-let-7f-1-3p	28.893	hsa-miR-17-3p	34.352
hsa-miR-33a-5p	28.953	hsa-miR-551b-5p	34.363
hsa-miR-1254	28.972	hsa-miR-604	34.392
hsa-miR-1227-3p	28.979	hsa-miR-643	34.461
hsa-miR-363-5p	29.141	hsa-miR-30c-1-3p	34.473
hsa-miR-138-2-3p	29.307	hsa-miR-26a-2-3p	34.708
hsa-miR-29b-2-5p	29.315	hsa-miR-668-3p	3.4709
hsa-miR-181a-3p	29.466	hsa-miR-937-3p	34.753
hsa-miR-744-3p	29.599	hsa-miR-1263	34.754
hsa-let-7b-3p	29.606	hsa-miR-624-5p	34.803
hsa-miR-126-5p	29.614	hsa-miR-516-3p	34.869
hsa-miR-1825	2.9637	hsa-miR-549a	34.978
hsa-miR-25-5p	29.786	hsa-miR-601	35.067
hsa-miR-1298-5p	29.791	hsa-miR-374b-3p	35.166
hsa-miR-1285-3p	29.895	hsa-miR-302a-5p	35.169
hsa-miR-7-2-3p	29.977	hsa-miR-1243	35.272
hsa-miR-21-3p	30.145	hsa-miR-432-3p	3.5274
		hsa-miR-767-5p	35.630

Supplemental Table 2. Mean CT values of the 10 most expressed miRNAs in uEVs evaluated by qRT-PCR. Data are mean ±SD of three different experiments using three different EV pools.

uEVs	CT	SD
hsa-miR-30a-3p	23.80	±0.14
hsa-miR-30e-3p	24.73	±0.18
hsa-miR-30a-5p	19.89	±0.04
hsa-miR-30d-3p	29.73	±0.18
hsa-miR-10b-3p	31.71	±0.19
hsa-miR-664a-3p	25.99	±0.22
hsa-miR-151a-3p	26.87	±0.05
hsa-miR-1260a	20.33	±0.37
hsa-miR-31-3p	32.61	±0.29
hsa-miR-151a-5p	24.68	±0.22
RNU6B	28.28	±0.47